HOKKAIDO UNIVERSITY

Title	Magma dynamics and collapse mechanisms during four historic caldera-forming events
Author(s)	Stix, John; Kobayashi, Tomokazu
Citation	Journal of Geophysical Research. B, Solid earth, 113(9), B09205 https://doi.org/10.1029/2007JB005073
Issue Date	2008-09-04
Doc URL	https://hdl.handle.net/2115/34998
Rights	An edited version of this paper was published by AGU. Copyright 2008 American Geophysical Union.
Type	journal article
File Information	Stix_Kobayashi_JGR2008.pdf

Hokkaido University Collection of Scholarly and Academic Papers : HUSCAP

Magma dynamics and collapse mechanisms during four historic caldera-forming events

John Stix, Department of Earth and Planetary Sciences, McGill University, 3450 University Street, Montreal, Quebec H3A 2A7, Canada

Tel +1-514-398-5391, Fax +1-514-398-4680, Email stix@eps.mcgill.ca

Tomokazu Kobayashi, Institute of Seismology and Volcanology, Graduate School of Science, Hokkaido University, Kita 10 Nishi 8, Kita-ku, Sapporo, 060-0810, Japan

Tel +81-11-706-3552, Email tkoba@uvo.sci.hokudai.ac.jp

Abstract

Four historic caldera-forming events were studied to understand the relationship of magma withdrawal processes and caldera subsidence mechanisms. Two calderas are silicic (Katmai 1912, Pinatubo 1991) and two are basaltic (Fernandina 1968, Miyakejima 2000). All events have sufficient geophysical, geologic, and petrologic data with which to examine and model magma withdrawal and caldera collapse. The data reveal that the magmas erupted at Katmai and Pinatubo were in a bubbly state in the reservoir immediately before and during caldera collapse. The bubbly magma allowed for its efficient extraction from the reservoir, causing significant underpressures to develop rapidly, particularly in the case of Katmai where the erupted rhyolite was voluminous, nearly aphyric, and very low viscosity. The rapidly developing underpressures at Katmai and Pinatubo caused sudden en masse caldera collapse halfway through the climactic eruptions, thereby liberating large amounts of seismic energy. At Fernandina and Miyakejima, by contrast, caldera collapse was initiated early and continued for an

extended period of time from weeks to months, consisting of a series of discrete subsidence events manifested by large earthquakes at Fernandina and by very long period (VLP) signals at Miyakejima. Systematic changes in earthquake magnitudes and quiescent intervals at both volcanoes reveal changes in friction as collapse took place during extended time intervals.

1. Introduction

Our understanding of calderas has increased significantly in recent years. This improvement is the result of new experimental and theoretical research which has complemented detailed field studies of calderas. By marrying these different approaches, we have gained important insight into the surface and subsurface workings of caldera systems. Experiments by *Roche et al.* [2000] have shown, for example, that the aspect ratio of the roof (thickness/width) plays an important role for the style of caldera collapse, with piston-style behavior at low aspect ratios and more piecemeal collapse at larger aspect ratios, often accompanied by subsurface stoping. *Roche and Druitt* [2001] developed a failure criterion for piston collapse which is related to the aspect ratio of the roof. Experiments by *Kennedy et al.* [2004] showed that many calderas are polygonal in nature rather than circular, due in part to crustal heterogeneities. Modelling by *Folch and Martí* [1998] and *Martí et al.* [2000] examined pressure variations during caldera-forming eruptions, while *Legros et al.* [2000] studied the effect of changing conduit geometry upon such large-scale eruptions. *Kumagai et al.* [2001] developed a pumping model of caldera subsidence, whereby changing pressures in the reservoir controlled the style and amount of subsidence.

Despite these impressive advances, there are a number of important unresolved questions regarding caldera formation. Perhaps most importantly, the timing of collapse is not well known for real calderas. Does subsidence begin at an early stage during the eruption, or does it commence at a later stage? Does subsidence occur in a continuous or incremental fashion throughout the eruption, or does it occur suddenly and en masse at some specific time? The aspect ratio of the roof may play an important role in the timing, with small values favoring early and/or incremental collapse, and large values resulting in late-stage en masse subsidence. The occurrence of lithic lag breccias interbedded with ignimbrite deposits can help shed light on the timing of collapse [e.g., *Druitt and Bacon*, 1986]. Nevertheless, our understanding of this problem is still rudimentary. A second related issue is the relationship between magma withdrawal and caldera collapse. This question is important, since it bears upon the amount of underpressure, due to withdrawal of magma, which develops in the magma reservoir before the onset of subsidence. Third, the issue of collapse dynamics is still unresolved. Does subsidence occur as a response to magma withdrawal from the reservoir? Or does subsidence of the roof forcefully push magma out of the reservoir, in the process repressurizing the system [*Druitt and Sparks*, 1984; *Martí et al*., 2000; *Kumagai et al*., 2001]? Finally, what is the effect of magma rheology upon the magma extraction and subsidence processes? For example, magmas that are poor in crystals may behave differently during their extraction compared to crystal-rich magmas. The extent to which a magma is compressible also may influence the amount of underpressure that develops due to magma withdrawal.

The purpose of this report is to explore these issues by examining four historic caldera-forming events which are well-documented and have adequate geologic and

76 geophysical data with which to address these questions. Of the four, two are silicic
77 eruptions (Katmai 1912, Pinatubo 1991) and two are mafic (Fernandina 1968,
78 Miyakejima 2000), thus providing both compositional similarities and contrast. For each
79 example, the process of magma extraction is examined in relation to caldera collapse, as
80 manifested by seismicity which was recorded at the time. Additionally, the magma
81 rheology and dynamics are analyzed to study their effects upon underpressure generated
82 by magma extraction, as well as upon the subsequent subsidence. The goal is to shed
83 light on these and related issues by integrating observational, experimental, and
84 theoretical data related to caldera formation.
85

86 ## 2. Chronology of Caldera Development

87 ### 2.1. Katmai 1912

88 Much of the following summary of the 1912 Katmai eruption draws upon the
89 important papers by *Abe* [1992] and *Hildreth and Fierstein* [2000]. The climactic
90 eruption of Katmai lasted 60 hours and erupted 13.5 km^3 of magma (dense rock
91 equivalent or DRE), frequently with simultaneous plinian and ignimbrite activity. The
92 eruptive materials consisted of nearly aphyric rhyolite (7-8 km^3 DRE), dacite (4.5 km^3),
93 and andesite (1 km^3), both with 30-50% crystals. The rhyolite was erupted at the
94 beginning of the eruption and was predominant. The aspect ratio of the magma
95 reservoir's roof was approximately 2, based on a thickness of 4-5 km and an average
96 width of 2.3 km [*Hildreth and Fierstein*, 2000] (Table 1).

97 A critically important phase of the climactic eruption occurred at about 1000 UTC
98 on 7 June (midnight local time on 6 June, the time difference being 10 hours), about 11

hours after the onset of the eruption. To this point, a cumulative amount of ~8.7 km^3 DRE of magma had been erupted, representing 64% of the 13.5 km^3 total volume, with an average evacuation rate of ~2.2 x 10^5 m^3 s^{-1}. This 8.7 km^3 volume was nearly all rhyolite; at this point in time, however, the relative proportions changed dramatically, with rhyolite decreasing to 40-50% and dacite and andesite increasing to ~40% and ~10%, respectively. Subsequently, the evacuation rate declined abruptly to ~2.8 x 10^4 m^3 s^{-1} well into 8 June. For a period of 5-6 hours on 7 June, the relative proportions of the three magma types fluctuated rapidly and substantially.

Seismicity during the climactic eruption was characterized by very high levels of liberated energy, mainly due to several large-magnitude earthquakes [*Abe*, 1992; *Hildreth and Fierstein*, 2000]. The pattern of seismicity exhibited several large, rapid jumps when plotted on a diagram of cumulative energy vs. time (Fig. 1a). Energies were calculated as $\log E = 1.96 M + 2.05$ where E is the energy in Joules and M the magnitude of the earthquake. The first significant increase occurred at 0956 UTC on 7 June, with a M 6.5 earthquake coinciding with the change in magma compositions described above. This event may indicate the initiation of caldera collapse, since the first lithic mud layer was erupted from the volcano at this time, followed by a second mud layer approximately six hours later [*Hildreth and Fierstein*, 2000]. The second major jump began with a M 7.0 earthquake at 0736 UTC on 8 June, followed by a M 6.8 event at 0848 UTC and a M 6.6 event at 1300 UTC [Abe, 1992] (Fig. 1a). During this 5½ hour period, approximately 60% of the total energy associated with the climactic eruption was released, likely corresponding with the bulk of caldera subsidence [*Hildreth and Fierstein*, 2000].

We have redrawn Figure 1 as a non-dimensional diagram (Fig. 2) where time is normalized to the duration of the climactic eruption, and cumulative energy is normalized to the total energy released during and immediately after the climactic eruption. At Katmai, there is a clear mismatch between erupted magma and released seismic energy during the climactic eruption, with significant amounts of magma being erupted well before the bulk of the seismic energy release (Fig. 2a). For example, by the first M 6.5 earthquake at 0956 UTC on 7 June, ~64% of the total magma volume had already been erupted, while only ~4.5% of the cumulative seismic energy was released. At this stage, the eruption was less than 20% complete. By the time of the M 7.0 earthquake at 0736 UTC on 8 June, approximately halfway through the climactic eruption, 80% of the magma had been erupted and 51% of the seismic energy released.

A final point is that of the total released seismic energy associated with caldera collapse at Katmai, 74% was released during the 60-hour climactic eruption. Thus, there was additional seismic energy released after the climactic eruption, which may be related to structural adjustments and further collapse of the unstable edifice.

2.2 Pinatubo 1991

The climactic phase of the 15 June 1991 Pinatubo eruption lasted approximately 8.8 hours, beginning at 0542 UTC (1342 local time, the time difference being 8 hours) [*Hoblitt et al*., 1996]. The eruptive products consisted almost entirely of dacite, with 3.7-5.3 km^3 of DRE magma erupted [*Scott et al*., 1996]. According to these values, the mean magma discharge rate ranged from 1.2 x 10^5 m^3 s^{-1} to 1.7 x 10^5 m^3 s^{-1}. *Koyaguchi and Ohno* [2001] have suggested that initial discharge rates may have reached as high as 3.6 x

144 10^5 m^3 s^{-1}, subsequently declining to ~1.2 x 10^5 m^3 s^{-1} during the course of the eruption.
145 The aspect ratio of the roof was ~2.4, based upon the observed caldera diameter of 2.5
146 km and depth to the top of the magma reservoir of ~6 km [*Mori et al*., 1996a; *Rutherford*
147 *and Devine*, 1996] (Table 1). This is a maximum value, as the lateral extent of the roof
148 may have been greater at depth.

149 Significant seismicity began with a M 5.1 event at 0739 UTC on 15 June, two
150 hours after the the beginning of the climactic eruption [*Mori et al*., 1996b]. The pattern of
151 cumulative seismic energy resembles that of Katmai, with large jumps occurring midway
152 through the eruption (Fig. 1b). At 1041 UTC, a M 5.5 event was recorded, and 34
153 minutes later at 1115 UTC, the largest earthquake of the sequence (M 5.7) was observed.
154 The bulk of caldera collapse may have occurred at the time of these large-magnitude
155 events [*Scott et al*., 1996], although there is some uncertainty as to whether the
156 earthquakes were related directly to collapse or were tectonic in origin [*Bautista et al*.,
157 1996]. Lithic breccias and lithic-rich pyroclastic flow deposits were observed to overlie
158 most of the pumiceous pyroclastic flow deposits [*Scott et al.*, 1996], also suggesting that
159 the majority of collapse took place at a relatively late stage during the climactic eruption.

160 Similar to Katmai, there is a mismatch in timing between erupted magma and
161 released seismic energy (Fig. 2b). By the time of the M 5.5 earthquake at 1041 UTC, at
162 least 57% of the total magma volume of 3.7-5.3 km^3 had been erupted, while only 14% of
163 cumulative energy was released. The value of 57% may in fact be appreciably larger if
164 discharge rates were high during early stages of the climactic eruption, as suggested by
165 *Koyaguchi and Ohno* [2001]. When the M 5.7 event occurred at 1115 UTC, at least 63%

of the magma had been erupted, with 43% of the cumulative energy released. At this stage, the climactic eruption was nearly two thirds complete.

Compared to Katmai, proportionally more seismic energy was released at Pinatubo after the climactic eruption stopped (51% for Pinatubo vs. 26% for Katmai) than during the eruption itself. Discharge rates at Pinatubo appear to be higher than at Katmai, while the climactic eruption was significantly shorter. As a result, structural adjustments after the climactic eruption may have been more significant at Pinatubo than at Katmai.

2.3 Fernandina 1968

By contrast with Katmai and Pinatubo, caldera development at Fernandina in 1968 occurred over an extended period of 250-300 hours between 12-21 June [*Simkin and Howard*, 1970; *Filson et al*., 1973]. The magma was basaltic in composition. Nearly all magma displacement occurred beneath the surface, with only a small amount erupted. A caldera was already present when this collapse episode took place. During 12-21 June 1968, the caldera floor subsided a maximum of 350 m in the southeast sector. A pre-existing tuff cone on the caldera floor was observed to be undisturbed after the collapse event [*Simkin and Howard*, 1970; *Filson et al*., 1973]. These observations suggest trapdoor-style piston subsidence. The new collapse volume at the surface was 2.0-2.4 km^3. Based upon a 1 km-thick roof and a 3200 m equivalent diameter of the caldera floor, the aspect ratio of the roof was ~0.3 (Table 1), although there is some uncertainty of the roof thickness [*Filson et al*., 1973].

The sequence of events began with an eruption accompanied by lava flows which were observed on the eastern flank of the volcano on 21 May 1968. A possible explosion

189 occurred on 8 June at 0220 UTC (2020 local time on 7 June, the time difference being 6
190 hours). On 11 June, a vapor cloud was observed after a M 3 earthquake at 1618 UTC.
191 This emission was followed by two large explosive eruptions at 2218 and 2308 UTC
192 which may have been partly phreatomagmatic [*Simkin and Howard*, 1970; *Filson et al*.,
193 1973]. After these events, significant amounts of lithic-rich tephra began to fall, an
194 occurrence which may have marked the initiation of caldera collapse [*Simkin and*
195 *Howard*, 1970]. Eruptive activity then diminished on 12 June, while seismic activity
196 increased, with a series of $M \geq 5$ earthquakes beginning at 2221 UTC [*Filson et al*.,
197 1973]. These large earthquakes probably represented the early stages of caldera
198 subsidence. Mean minimum magma evacuation rates were 3.0-3.4 x 10^3 m^3 s^{-1}, based on
199 a caldera collapse volume of 2.2 x 10^9 m^3 and a duration of 182 hours from 12-20 June
200 for subsurface drainage of magma from the reservoir. These rates are several orders of
201 magnitude less than at Katmai and Pinatubo.
202 The seismicity associated with collapse at Fernandina was exceptional [*Filson et*
203 *al*., 1973]. From 2221 UTC on 12 June to 0420 UTC on 15 June, there were a series of M
204 ≥ 5 events which were regularly spaced at ~6 hours. Beginning at 0851 UTC on 15 June,
205 the large events decreased (a) in magnitude to M 4.7-4.9 and (b) in spacing to ~4-hour
206 intervals. Starting late on 16 June or early on 17 June, the seismic pattern changed yet
207 again, with more closely spaced events of generally smaller magnitudes (i.e., M 4.0-4.5).
208 At about 1200 UTC on 20 June, the number of earthquakes decreased rapidly. For
209 example, 89 events were recorded on 20 June, 13 on 23 June, and only 5 on 24 June
210 [*Filson et al*., 1973]. Recorded seismicity stopped on 27 July.

By contrast with Katmai and Pinatubo, the overall pattern of seismic energy released by Fernandina during caldera subsidence was quite regular, showing initially high rates of energy which gradually subsided with time to zero (Fig. 1c). The trend between 25-75 hours is charaterized by a series of abrupt jumps, which are the M 5 events occurring mainly on 13-14 June. The jumps then become smaller and eventually indiscernible on the diagram by 150 hours as earthquakes diminished in magnitude and increased in number.

2.4 Miyakejima 2000

Caldera development at Miyakejima from 8 July of 2000 was even more protracted than at Fernandina, extending over a period of about 40 days. However, the nature of magma evacuation at Miyakejima resembled that at Fernandina. The total volume of the caldera of 6 x 10^8 m^3 [*Geshi et al.*, 2002] is much larger than the volume of ejecta from the eruption (9.3 x 10^6 m^3) [*Nakada et al.*, 2005], since magma was displaced almost entirely in the subsurface, with very little material being erupted. The caldera was intermittently enlarged during July-August 2000, and its final size was 1.6 km in diameter and 450 m in depth [*Geshi et al.*, 2002]. The depth of the magma chamber related to caldera formation is not well-known, but seismic and geodetic surveys suggest that a pressure source is located at a depth of 3-6 km [*Kobayashi et al.*, 2003; *Irwan et al.*, 2003; *Ueda et al.*, 2005]. Using 3-6 km as the thickness of the caldera block, the aspect ratio of the roof is evaluated as 1.9 ~ 3.8.

The magmatic activity began with a gigantic seismic swarm on 26 June around 0859 UTC (1759 local time on 26 June, the time difference being 9 hours) [*Ueda et al.*,

234 2005; *Uhira et al.*, 2005] caused by northwestward dike-forming intrusions of magma,
235 followed by a small submarine eruption [*Nakada et al.*, 2005; *Kaneko et al.*, 2005]. The
236 earthquake swarm beneath the island died out by the next day, and activity shifted to a
237 comparatively quiescent stage. However, small volcanic earthquakes began to be
238 recorded beneath the summit at the beginning of July, leading to a summit eruption on 8
239 July at 0941 UTC, accompanied by significant subsidence at the surface. A void was
240 already present just beneath the summit several days before the first summit eruption, so
241 that the subsidence on 8 July is interpreted as collapse of a block into a shallow void
242 space [*Furuya et al.*, 2003]. The caldera grew incrementally after the eruption [*Geshi et*
243 *al*., 2002], with infrequent explosive eruptions. The caldera had grown to about 1.5 km in
244 diameter by early August and was widened later by landslides off its steep walls [*Nakada*
245 *et al.*, 2005]. Intermittent explosive eruptions that had occurred from 10 August
246 eventually led to the largest explosion on 18 August around 0900 UTC which was
247 vulcanian to subplinian in nature. After this eruption, significant caldera development
248 was not observed. The caldera size finally reached ~0.6 km^3 in volume [*Geshi et al*.,
249 2000]. Based on the duration between the first summit subsidence on 8 July and the
250 largest eruption on 18 August (984 hours), the mean magma evacuation rate is estimated
251 at ~170 m^3 s^{-1}. The rate is significantly less than the other three volcanoes. After the
252 largest eruption, the characteristic activity was strong degassing. By the end of August
253 and early September, the volcano began to emit substantial quantities of sulfur dioxide, at
254 times exceeding 100,000 metric tonnes SO_2 per day [*Kazahaya et al*., 2004].
255 The seismic activity during caldera formation was characterized by very long-
256 period (VLP) seismic pulses having a pulse width of about 50 seconds [*Kikuchi et al.*,

2001; *Kumagai et al.,* 2001]. A series of VLP signals were observed once or twice a day from 9 July at 1339 UTC to 17 August at 1907 UTC. This period corresponds exactly with the observed duration of caldera development. The equivalent moment magnitudes are 5.0 to 5.6, according to *Kikuchi et al.* [2001]. In addition to the VLP signals, other earthquakes occurred during the caldera formation stage, e.g., series of earthquakes which were observed as precursors to the VLP signal [*Kobayashi et al.*, 2003], but the magnitude of these individual events was only 1 to 2. Thus, the total released seismic energy during caldera development can be generally described by the VLP signals alone (Fig. 3). The released seismic energy of each VLP event is calculated as $\log E_s = \log M_0 - 4.3$, where the seismic energy E_s is in Joules and the seismic moment M_0 is in Nm. The overall trend of released seismic energy is similar to that of Fernandina; the seismic energy was regularly released at a nearly constant rate, unlike the pattern of Katmai and Pinatubo. In early stages, the occurrence interval was approximately 12 h, but it became substantially longer at the beginning of August (~500 h on Fig. 3), with magnitudes of individual VLP events correspondingly increasing. This trend of occurrence is opposite to the case of Fernandina. The repetitious character of these VLP signals, as well as the constant growth rate of the caldera, implies that the subsidence process at Miyakejima was highly regular and systematic. *Kumagai et al*. [2001] have interpreted these signals as a volumetric expansion of the magma reservoir which may be associated with slip of a vertical piston in the conduit, followed by magma outflow and gradual depressurization. Slow deflation was recorded by the tiltmeters on the island [e.g., *Ukawa et al.*, 2000] during the interval of VLP occurrence representing rapid short-term inflations of the magma reservoir. Thus, these seismic events can describe a basic framework of magma

withdrawal on short timescales controlling caldera development, a process which is superimposed upon deformation trends at longer timescales. This may be a common feature for other volcanoes as well.

3. Modelling the Subsidence Process

The high aspect ratios of the Katmai and Pinatubo caldera blocks illustrate the presence of comparatively thick crust which likely provided "bridging" roof support for the magma reservoirs beneath. Accordingly, Katmai and Pinatubo illustrate the mismatch between early magma withdrawal and comparatively late caldera collapse. By contrast, magma withdrawal and caldera subsidence at Fernandina and Miyakejima appear to have taken place during short intervals and in a progressive manner. In the case of Fernandina, the thin roof may not have provided much support or resistance before or during subsidence. Miyakejima is a more complicated case which exhibited both a thin roof during initial caldera collapse [*Kikuchi et al.*, 2001], as well as a thicker crustal block which subsided in a progressive fashion during the summer of 2000. These differences pose interesting questions regarding the properties of the magmas, the nature of the magma withdrawal process, and the dynamics of caldera formation during these eruptions.

Because the eruptions have been well studied, many parameters relating to the eruptions are well constrained, and the eruptions thus can be modeled with some confidence in terms of magma withdrawal and caldera development. *Kumagai et al*. [2001] have modeled caldera subsidence at Miyakejima in the middle of 2000. Their approach can be adapted for use at Katmai, Pinatubo, and Fernandina with certain caveats, in particular that caldera subsidence occurs as a piston-style process. By this, we

mean that the roof of the magma reservoir subsided coherently as a single block. This style of subsidence is illustrated schematically in Figure 4. We recognize that many calderas have more complicated subsidence styles, such as piecemeal, downsagging, a series of concentric downthrown blocks, etc. [*Kennedy and Stix*, 2003]. Nevertheless, while this collapse style is likely an oversimplification, it is sufficient for the modelling presented here, since Katmai and Pinatubo collapsed en masse and Fernandina and Miyakejima as a series of discrete steps. *Kumagai et al*. [2001] show that the piston begins to move downward after a time T:

$$T = \frac{2(F_s - F_d)}{p'A} \qquad (1)$$

where $F_s - F_d$ are static and dynamic frictions, respectively, p' is the rate of pressure decrease due to outflow of magma from the magma chamber, and A is the cross-sectional area at the base of the piston (all symbols are explained in Table 2). Equation (1) can be rewritten as

$$p'TA > 2(F_s - F_d) \qquad (2)$$

which shows that the piston will move downward when the pressure decrease $p'T$ exceeds the rock friction or rock strength. *Kumagai et al*.'s [2001] model is essentially one of repeatedly pumping the magma chamber with the piston:

$$p_1 = p_0 - p'T + p \qquad (3)$$

where p_0 is the original pressure in the magma chamber, $p'T$ is the pressure decrease due to magma outflow, p is the pressure increase in the chamber once the caldera block begins to move downward, and p_1 is the re-equilibrated pressure in the magma chamber. The equation describes a stick-slip sense of movement of the caldera block, where stick is associated with underpressure as magma is erupted or drained from the reservoir. After a certain time, underpressure exceeds friction, and the block begins to slip. This movement may squeeze the magma, causing it to be repressured. Equation (3) can be written as

$$p_1 = p_0 + \kappa[(-\alpha T + Az) / V_0] \qquad (4)$$

where κ is the bulk modulus of the magma, α the evacuation rate of the magma, z the displacement of the block, and V_0 the initial volume of the magma chamber before caldera subsidence is initiated [*Kumagai et al*., 2001].

With respect to events at Katmai and Pinatubo, we are interested primarily in pressure variations of the magma reservoir before the bulk of collapse occurred. As observed in Figures 1-2 above, there was an extended period of magma withdrawal before the bulk of collapse was initiated approximately halfway through the climactic eruptions, as manifested by the sudden onset of large-scale seismicity. This period of magma withdrawal indicates that pressure was decreasing in the magma reservoirs at both volcanoes. The pressure decrease prior to caldera subsidence can be calculated as follows:

$$p'T = \frac{\kappa\alpha T}{V_0} \qquad (5)$$

For Katmai and Pinatubo, we assume that the bulk of collapse occurred in a short time interval about halfway through the climactic eruption. For Fernandina, collapse occurred incrementally separated by quiescent intervals of six hours. The parameters T, α, and V_0 are reasonably constrained at all three volcanoes (Table 1), while κ is not. Therefore, we have plotted the pressure decrease against a range of bulk moduli in Figure 5. For Katmai and Pinatubo, bulk moduli range from ~10^6 Pa to 10^{10} Pa for pressure decreases from 1 MPa to nearly 10 GPa, respectively.

Equations (2) and (5) are valid once the caldera collapse process is in a steady-state condition, i.e., the caldera block is alternately sticking and slipping during the course of subsidence. At Katmai and Pinatubo, however, this condition may not be strictly true, as the evacuating magma reservoir and increasing underpressure were developing before the bulk of subsidence was initiated. Here, the resistance to subsidence was provided by the shear strength and fracture processes of the country rocks. In this case, an independent approach for estimating underpressures is to use the failure criterion method of *Roche and Druitt* [2001], which calculates the underpressure $p'T_{crit}$ which is required to exceed a critical shear stress upon the rocks above the magma reservoir:

$$p'T_{crit} \geq 4R\tau_c \qquad (6)$$

where R is the aspect ratio of the caldera block as defined by its thickness H divided by its diameter D, and τ_c is the critical shear stress for failure. This shear stress can be solved as follows:

$$\tau_c = \tau_o + \mu\sigma_n \qquad (7)$$

where τ_o is the cohesion of the caldera block, μ is the coefficient of internal friction of the block (~0.6) [*Byerlee*, 1978], and σ_n is the mean stress normal to the plane of failure. This last parameter can be calculated as $\sigma_n = kp_{lith}$ where k is a constant (~0.6) [*Cornet and Valette*, 1984], p_{lith} is the lithostatic pressure $\rho_r gH/2$, ρ_r is the average density of the caldera block, and g is the acceleration due to gravity.

Using these equations gives underpressures of 166-205 MPa for Katmai and 265-312 MPa for Pinatubo for a range of cohesions from 0.1 MPa to 5 MPa [*Roche and Druitt,* 2001]. These values may be overestimates, as shear strengths of rocks beneath volcanoes are typically on the order of 1-100 MPa [*Martí et al.,* 2000]. Nevertheless, these calculations provide a useful upper limit of underpressures at these two volcanoes, while our calculations from Equation (5) use a lower limit of 1 MPa. For these levels of underpressure, therefore, bulk moduli for Katmai range from a low of 1.2×10^6 Pa to a high of $2.0\text{-}2.5 \times 10^8$ Pa, while for Pinatubo the range is from 2.0×10^6 Pa to $5.2\text{-}6.1 \times 10^8$ Pa (Fig. 5). The bulk modulus for bubble-free magma is $\sim 10^{10}$ Pa, while that for bubbly magma is typically $10^7\text{-}10^9$ Pa [*Huppert and Woods*, 2002]. It is thus reasonable to conclude that reservoir magmas at Katmai and Pinatubo were bubbly immediately before and during caldera collapse.

For Fernandina, the case is less clear, as pressure decreases range from ~0.3 MPa to ~290 MPa for bulk moduli of 10^7-10^{10} Pa (Fig. 5). This large range can be further constrained by the approach of *Roche and Druitt* [2001], as done above for Katmai and Pinatubo, and these calculations result in maximum critical underpressures of 3-9 MPa for Fernandina using the same range of cohesions as above. The comparatively low magma evacuation rates at Fernandina (10^3 m^3 s^{-1} compared to 10^4-10^5 m^3 s^{-1} at Katmai and Pinatubo) also imply relatively small amounts of underpressure. Thus, we suggest that the basaltic magma in the reservoir beneath Fernandina also had a reduced bulk modulus and appreciable vesicularity as it drained in the subsurface (Fig. 5).

It is important to assess the quality of the values we have used in these underpressure calculations, in particular the parameters T, α, and V_0 (Table 1). In the case of T, we are fairly confident of the data, since they are constrained (1) by the time between the start of the climactic eruption and the sudden onset of large-scale seismicity for Katmai and Pinatubo, or (2) by the periods of seismic quiet between major earthquakes at Fernandina. For α, the values we have used for Katmai and Pinatubo appear reasonable, as they are constrained by the volume of magma erupted during the course of the climactic eruption divided by its duration. Further refinements based on field studies have been possible for both volcanoes [*Hildreth and Fierstein,* 2000; *Koyaguchi and Ohno,* 2001]. For Fernandina, the case is not so clear because very little magma was erupted. Thus, we have used the caldera collapse volume at the surface divided by the duration of the collapse events. This is probably a minimum rate, so we have doubled this value to provide an upper limit. Lastly, the V_0 parameter is not particularly well constrained. Thus we have simply used the volumes of erupted magma

(Katmai, Pinatubo) or caldera collapse volume (Fernandina) to represent V_0. These are clearly minimum values; however, larger values of V_0 would result in decreased underpressures and bulk moduli (Fig. 5), reinforcing the argument that the magmas were bubbly upon evacuation. A magma reservoir which empties itself entirely during a climactic eruption is an interesting concept [*Martí et al.,* 2000]. Such conditions might promote its replenishment during and/or immediately after the eruption [e.g., *Stix and Gorton,* 1993]. Another possibility is a larger magma reservoir in which the largely liquid portion is erupted while the more crystallized portion is not.

In these calculations, the T parameter is of crucial importance, since it is directly related to the amount of underpressure that is generated before the roof fails and the bulk of caldera collapse is initiated. It is thus essential to know if the T parameter is being used appropriately and correctly in the calculations above. This can be verified by calculating the displacement of the subsiding caldera block as follows. If T is significantly longer than the duration of piston displacement, as appears to be the case for Katmai and Pinatubo and probably Fernandina as well (Figs. 1, 2), then the displacement of the caldera block can be estimated thus:

$$z = \alpha T / A \qquad (8)$$

Results for Katmai and Pinatubo are shown in Figure 6 and Table 3. Since magma evacuation rates likely varied during the course of the climactic eruptions, we have used a range of values from the minimum and maximum estimates. Allowing for some

uncertainty in the magma evacuation rates, the agreement between calculated and observed displacements is good (Table 3).

Equation (8) also can be used to examine the nature of subsidence at Fernandina. In this case, *T* and *A* are known while α is not. Figure 7 shows the effects of evacuation rate and time before subsidence on the amount of displacement of the piston. For evacuation rates ranging from a minimum of 2970 m^3 s^{-1} to a maximum of 6730 m^3 s^{-1}, individual displacements are 8-18 m, respectively. Notably, the spacing between major earthquakes changed on 15 June from 6 hours to 4 hours, with a corresponding decrease in the magnitudes of the earthquakes. Inputting these intervals as values for *T* reveals that individual displacements, as manifested by the earthquakes, decreased on 15 June from 8.0 m to 5.4 m, using a constant evacuation rate of 2970 m^3 s^{-1}. In summary, it is certain that (a) subsidence at Fernandina was incremental, in contrast to Katmai and Pinatubo, and (b) the amount of displacement for individual subsidence events declined with time. It is possible that both declining evacuation rates and time intervals between earthquakes contributed to these decreasing displacements. Alternatively, the evacuation rate remained approximately constant, and the smaller displacements were the result of reduced time intervals between earthquakes. This issue is examined more fully in the next section.

4. Discussion

The analysis above has relevance for the dynamics of magma extraction, the nature of caldera subsidence, the presence of bubbly magma stored in shallow magma

464 reservoirs, and the progressive weakening of caldera faults. Furthermore, it is clear that in
465 many cases these issues are inter-related. These points are discussed in turn below.
466
467 **4.1 Early Extraction and Eruption of Silicic Magma at Katmai and Pinatubo**
468 The bulk of caldera collapse appears to have occurred midway through the
469 climactic eruptions at Katmai and Pinatubo. Most of the magma was withdrawn and
470 erupted rapidly in the early stages of the eruptions, allowing significant underpressures to
471 quickly develop in the magma reservoirs. The early-erupted magma was highly
472 extractable, principally due to its low viscosity. In the case of rhyolite magma at Katmai,
473 for example, viscosity calculations using the method of *Hess and Dingwell* [1996]
474 indicate that viscosities ranged from a maximum of 1.4×10^5 Pa s at 4 wt. % H_2O and
475 805° C to a minimum of 7.1×10^3 Pa s at 7 wt. % H_2O and 850º C [*Westrich et al*., 1991;
476 *Lowenstern*, 1993; *Cowee et al*., 1999; *Hildreth and Fierstein*, 2000; *Coombs and*
477 *Gardner*, 2001]. As magma transited the conduit, flow was likely shearing at high strain
478 rates. Under these conditions, viscosities would be lowered even further due to shear
479 thinning behavior induced by the presence of bubbles [*Stein and Spera*, 2002] and/or
480 viscous dissipation effects [*Lavallée et al.*, 2007]. It is therefore possible that the
481 viscosity of rhyolite magma at Katmai approached values as low as 10^3 Pa s, which is
482 similar to the viscosity of dry basalt [*Khitarov et al*., 1976]. These low viscosities thus
483 allowed rapid extraction of the early-erupted magma from the reservoir, causing high
484 underpressures to develop as shown by Equation (5). High magma extraction rates also
485 may have been aided by large pressure gradients due to the free gas phase and by large
486 conduit dimensions.

Equation (5) also reveals that there may be a delicate balance between the bulk modulus and evacuation rate of the magma as a system is underpressured. In order to maintain reasonable underpressures (~100 MPa), bubbly magmas of low bulk modulus may be associated with high magma evacuation rates while bubble-poor magmas of high bulk modulus may be extracted at lower evacuation rates [*Huppert and Woods*, 2002].

At Katmai, a rheological interface was reached in the magma chamber at an early stage in the eruption when significant amounts of mixed crystal-rich dacite and andesite began to be erupted at ~1000 UTC on 7 June. Significant seismicity was initiated at this point, while the volumetric eruption rate decreased by nearly an order of magnitude. These changes likely are the result of the eruption's tapping a rheological boundary between low-viscosity rhyolite above and high-viscosity dacite and andesite underneath. Using the underpressure arguments from above, the bulk modulus also may have changed abruptly at this boundary from low values in rhyolite to high values in dacite and andesite. The seismicity may indicate onset of caldera collapse; if so, subsidence of the caldera block may have helped mix dacite and andesite.

Rheological boundaries in silicic magma chambers may be common occurrences, serving to slow or stop the course of an eruption [*Smith*, 1979, *Bacon and Druitt*, 1988; *Scaillet et al*., 1998; *Hildreth*, 2004]. At the 121 Ma Ossipee ring complex in New Hampshire, *Kennedy and Stix* [2007] have shown that crystal-poor rhyolite was erupted, resulting in caldera subsidence. After collapse, crystal-rich quartz syenites were intruded into the ring dyke. The magma chamber configuration thus consisted of low-viscosity rhyolite magma which was erupted from the top of the reservoir, underlain by high-viscosity quartz syenite crystal mush which was not extractable and not erupted.

In summary, magma rheology and rheological boundaries appear to strongly influence the course of caldera-forming eruptions. For such systems, the nature of magma extraction has profound implications for the timing and nature of caldera subsidence.

4.2 Magma Extraction, Caldera Subsidence, and Seismic Energy Release

Hildreth and Fierstein [2000] have shown that the seismic energy released at Katmai was 2-3 orders of magnitude higher than that observed at Pinatubo and Fernandina (and Miyakejima as well), attributing this difference to high-strength rocks, lateral magma flow, and horizontally layered structure at Katmai. As noted above, a comparatively large volume of magma was withdrawn and erupted at Katmai prior to the bulk of collapse. Experiments by *Roche et al*. [2000] and *Kennedy et al*. [2004] have shown that high aspect ratios of the caldera block result in late collapse after a significant volume of magma has been extracted from the reservoir. Such a situation allows large underpressures to develop in the reservoir before collapse is initiated. The experiments also reveal that subsidence occurs in a progressive fashion by stoping at low evacuation rates. In the case of high evacuation rates, however, we theorize that collapse may occur en masse after a significant proportion of magma has been withdrawn quickly from the reservoir, the subsidence involving a large fault surface area and significant slip. This style of collapse could be further facilitated by explosive enlargement of the ring fault or faults. In such a situation, the high seismic moment is principally the result of a large quantity of easily extractable magma which is erupted at a high rate from a deep reservoir, thus generating significant underpressure in a short period of time. The elevated evacuation rates result in a focusing of stress [*Sunde et al*., 2004], causing the

crust to fail catastrophically along major caldera faults. The ensuing caldera collapse occurs abruptly, releasing large amounts of seismic energy. If this hypothesis is correct, it implies that this style of collapse is closely linked to the depth of the magma reservoir, the magma's rheology, and the extraction rate of the magma.

4.3 Bubbly Magma in Shallow Reservoirs

The bulk modulus of a substance is a measure of its incompressibility. It is a balance between an imposed pressure difference and the associated volume change of the material:

$$\kappa = \frac{\Delta p}{\Delta V / V_0} \qquad (9)$$

Where Δp is the pressure difference and ΔV the change in volume. The calculations above demonstrate that the Katmai and Pinatubo reservoir magmas were in a bubbly state during their extraction prior to the bulk of caldera collapse. However, the calculations do not reveal the physical state of the magmas before the initiation of magma withdrawal. They may have been undersaturated, saturated, or oversaturated in volatiles. Other lines of evidence indicate that a pre-eruptive, separate fluid phase was present beneath Pinatubo [*Wallace and Gerlach*, 1994] and possibly Katmai [*Coombs and Gardner*, 2001; *Hammer et al*., 2002]. It is thus reasonable to infer that these magmas may have been partly vesicular before eruption, thereby aiding their extraction from the reservoir.

The occurrence of bubble-rich magma in shallow reservoirs has important ramifications for eruptive processes. Such magma will have high buoyancy and low

viscosity, particularly so if the magma contains few crystals; as a result, it will be mobile and easily extracted and erupted from the reservoir. These properties can explain the high eruption rates observed during the early stages of the Katmai and Pinatubo eruptions [*Hildreth and Fierstein*, 2000; *Koyaguchi and Ohno*, 2001] and are consistent with *Huppert and Woods'* [2002] model which shows enhanced eruption rates for magmas of low bulk modulus. Under these conditions, the rapid withdrawal of bubbly magma inevitably will lead to rapid fragmentation at deep levels in the conduit or even in the reservoir itself, since the fragmentation threshold is a sensitive function of vesicularity [*Spieler et al*., 2004].

The presence of bubbly magma also will allow efficient syn-eruptive release of volcanic gas [*Wallace et al*., 1995, 1999]. Silicic magmas, as exemplified by Katmai and Pinatubo, have a melt phase which is depleted in volatile components such as sulfur, and a free gas phase which is correspondingly enriched in these components. During eruptions, the volatiles will be released preferentially at an early stage, due to their buoyancy and concentration in the upper levels of the magma reservoir. This early release may be observable by remote sensing methods [*Rose et al*., 2000]. We hypothesize that many basaltic magmas also contain free gas in the upper parts of their subsurface plumbing. If so, these sulfur-rich systems may release large amounts of sulfur and other gases at the beginning of an explosive eruption [e.g., *Rose et al.*, 2003].

4.4 Modification of Caldera Faults During Subsidence at Fernandina and Miyakejima

By contrast with the sudden onset of caldera subsidence at Katmai and Pinatubo, collapse at Fernandina and Miyakejima was incremental and progressive. Fernandina and Miyakejima provide contrasting insight during caldera subsidence. At Fernandina, the patterns of seismic energy release can be grouped into discrete periods. For a given period, the interval of time between large earthquakes remained essentially constant, as did the magnitude of the earthquakes. The constant time interval implies that a critical stress value was attained repeatedly; once this level was reached, it was relieved by downward movement of the subsiding caldera block. The similar earthquake magnitudes suggest that (a) the block repeatedly subsided the same distance, as calculated above, and (b) the stress level returned to a common baseline value. The stress then started to build again during the next interval of time as magma continued to drain from the reservoir.

Notably at Fernandina, earthquake magnitudes and quiescent intervals both decreased abruptly after a period of time, best examplified at 0851 UTC on 15 June when large earthquakes decreased in magnitude from M $\geq$ 5 to M 4.7-4.9 and in spacing from ~6-hour to ~4-hour intervals. The concurrent decreases in both parameters strongly suggest that they are physically linked. The declining time interval can be expressed by Equation (1), which can be rewritten as

$$T = \frac{2V_0(F_s - F_d)}{\kappa\alpha A} \qquad (10)$$

where $p' = \kappa\alpha / V_0$. Here the important parameters are V_0, α, κ, and $F_s - F_d$, which are discussed in turn. As the caldera block subsided, the initial volume of the magma chamber V_0 was reduced; such a change should manifest itself by a continual decline in T.

605 This pattern was not observed, however, instead showing discrete periods of constant T
606 followed by a decline, as described above. A change in the magma's evacuation rate α
607 may also affect the value of T; a decrease of α would increase T, but the opposite
608 behavior is observed. An increase of α would lower T and result in greater displacements
609 of the subsiding caldera block and thus higher-magnitude earthquakes, but the opposite is
610 observed.

611 Increased values of κ would lower T as shown by Equation (10), implying that the
612 magma became less bubbly with time [*Filson et al.*, 1973]. This interesting possibility
613 suggests that the initially large subsidence events caused vesicular magma in the upper
614 parts of the reservoir to be compressed and pressurized reducing the amount of bubbles,
615 to a point where the caldera block stopped moving downward. Between subsidence
616 events, the reservoir drained, allowing magma beneath the caldera block to revesiculate
617 to an extent where the block again subsided. With time, decreasing volatile contents in
618 the magma reduced vesiculation, hence produced less subsidence and lower-magnitude
619 earthquakes. The relationship between increasing bulk modulus on the one hand and
620 reduced subsidence and smaller-magnitude seismicity on the other hand can be expressed
621 quantitatively thus:

622

623
624
625
$$z = \frac{2V_0(F_s - F_d)}{\kappa A^2} \qquad (11)$$

626

627 The shorter intervals between subsidence events may imply that evacuation rates
628 increased over time.

A second possibility is that $F_s - F_d$ declined during magma withdrawal and subsidence, causing T to decrease, as suggested originally by *Filson et al.* [1973] and examined recently by *Kobayashi et al.* [2003] at Miyakejima. Essentially, a lower critical stress threshold was reached sooner, and the block subsided. For a given evacuation rate, the shortened time interval between subsidence events resulted in smaller amounts of downward displacement of the caldera block. As a result, earthquake magnitudes also decreased. It appears that the friction forces resisting downward movement of the caldera block decreased with time in a stepwise fashion. This weakening process appears to have occurred at discrete intervals rather than as a continuous process.

A final view is that the caldera faults were inward dipping. As magma drained from the reservoir initially, the extent of collapse was comparatively large. As the magma continued to drain, however, the ability of the caldera block to subside diminished progressively due to the constricting faults. With time, the block became wedged between the faults, and subsidence ceased. This hypothesis is difficult to evaluate, as we have no direct evidence regarding the configuration of the caldera faults.

We can identify a similar temporal change of magnitude and time interval in the individual VLP events of Miyakejima, which provides complementary information for the understanding of frictional control. *Kobayashi et al*. [2003] have studied sequences of small-amplitude earthquakes, especially in the events at the beginning of the VLP activity, which were observed to occur about an hour before the appearance of a VLP signal. Initially, time intervals between these precursor earthquakes exhibited progressive and linear declines, while the earthquake amplitudes remained constant until near the end of a sequence when the amplitudes declined precipitously. To explain these patterns,

652 *Kobayashi et al*. [2003] use an asperity model where the caldera piston is strongly
653 coupled to the country rock by means of "asperites". The repeated earthquakes of similar
654 amplitude represent the progressive breaking of individual asperites which maintain
655 constant strength. As asperites break, the stress level returns to a baseline which then
656 increases more rapidly with time, since there are progressively fewer asperites holding
657 the block stationary against the country rock. Eventually, all asperites are broken, the
658 critical stress level declines rapidly to the baseline value, and the block starts to move.
659 This view of an individual subsidence event at Miyakejima shares similarities with the
660 sequence of subsidence events at Fernandina.

661 When examining the overall activity at Miyakejima, however, the temporal trends
662 provide a contrasting case to Fernandina. At Day ~500 about halfway through the events
663 of 2000 (Fig. 3), the time interval between successive VLP events increased, as did the
664 magnitudes and energies of individual VLP signals. This interesting observation is
665 exactly opposite to that seen for Fernandina. The seismic energy of a VLP signal is
666 related to an enhanced internal pressure of the magma chamber Δp, which can be
667 rewritten as $2V_0(F_s - F_d)/A$. Assuming that the A and V_0 parameters remain constant, the
668 friction parameter $(F_s - F_d)$ controls the temporal features in magnitude and time interval
669 simultaneously, suggesting that the effective friction on the caldera faults may have
670 increased in early August 2000. If this interpretation is correct, then a longer time
671 interval was required to reach the point of failure. If the magma evacuation rate remained
672 constant, the longer time interval implies that a greater amount of magma was drained
673 from the reservoir than previously occurred. Hence, the caldera block was able to fall
674 further during an individual subsidence event, producing a large-magnitude VLP signal.

675 In summary, for both Fernandina and Miyakejima, friction acting on the conduit wall
676 may play a pivotal role for the process of incremental subsidence of the piston.
677
678
679 **5. Conclusions**
680 The principal conclusions from this work are the following:
681 1. Caldera collapse at Katmai and Pinatubo occurred en masse at a comparatively late
682 stage in the course of the eruption, while subsidence at Fernandina and Miyakejima
683 proceeded incrementally. The en masse collapse was caused by the caldera block
684 subsiding in response to magma evacuation. By contrast, the incremental collapse
685 observed at the basaltic calderas may have resulted from the periodically subsiding
686 block forcefully pushing magma out of the reservoir.
687 2. During its evacuation, the magma in the reservoirs beneath Katmai and Pinatubo
688 possessed significant porosity and compressibility. Due to its compressibility and low
689 viscosity, the rhyolite magma at Katmai was easily extracted and erupted, leading to
690 significant underpressures prior to caldera subsidence.
691 3. At Katmai, changes in magma rheology appear to have played an important role in
692 magma withdrawal and timing of collapse. The development of underpressure may be
693 controlled by a delicate balance among certain parameters including the evacuation
694 rate of the magma, its bulk modulus, and its crystal content.
695 4. Incremental collapse at Fernandina and Miyakejima reveals contrasting behavior
696 which is probably related to modification of the caldera fault systems over the course
697 of protracted subsidence.

5. The amount of extractable and eruptable magma present in the reservoir determines, at least in part, the degree of underpressure in the reservoir, the evacuation rate of the magma, and the timing and style of caldera collapse. Such magmas possess low viscosities, small amounts of crystals, and substantial amounts of bubbles.

At Katmai and Pinatubo, magma discharge rates did not appear to increase when the bulk of subsidence occurred, since most of the ignimbrites had already been erupted before the major collapse episodes were initiated. Intracaldera ponding of ignimbrite does not appear to be significant at either volcano. For all four volcanoes studied here, the subsiding caldera blocks appear to have behaved coherently, either as pistons or as en masse subsidence. Aspect ratios of the caldera blocks for Katmai, Pinatubo, Miyakejima, and possibly Fernandina as well, may exceed those of larger caldera systems, where roof blocks may resemble thin plates. For these large systems, collapse may occur more incrementally and at an earlier stage due to the smaller aspect ratio. Incremental collapse promotes progressive ponding of ignimbrite, increasing the lithostatic load of the subsiding block. Thus, incremental collapse may result in an eruption style quite different from that associated with en masse collapse.

Acknowledgements. The starting point for this work began after reading Wes Hildreth and Judy Fierstein's fascinating paper on Katmai which they published in 2000. Events at Miyakejima volcano in 2000 also helped influence some of the ideas developed during our research. Comments by Ben Kennedy on an earlier version of the manuscript measurably improved the paper. Experimental work by Richard Sunde and Valérie

721 Frechette helped clarify some points regarding the role of magma evacuation rate on
722 caldera collapse. Formal reviews by Joan Martí and Hiroyuki Kumagai and comments by
723 Associate Editor Michael Ryan were inciteful, forcing us to rethink some of our ideas and
724 conclusions. This study was supported by an operating grant from the Natural Sciences
725 and Engineering Research Council of Canada and a team grant from Le Fonds québécois
726 de la recherche sur la nature et les technologies.

727

728 **References**

729 Abe, K. (1992), Seismicity of the caldera-making eruption of Mount Katmai, Alaska in
730 1912, *Bull. Seismol. Soc. Am., 82*, 175-191.

731 Bacon, C.R., and T. H. Druitt (1988), Compositional evolution of the zoned calcalkaline
732 magma chamber of Mount Mazama, Crater Lake, Oregon, *Contrib. Mineral. Petrol., 98*, 224-256.

734 Bautista, B. C., Ma. L. P. Bautista, R. S. Stein, E. S. Barcelona, R. S. Punongbayan, E. P.
735 Laguerta, A. R. Rasdas, G. Ambubuyog, and E. Q. Amin (1996), Relationship of
736 regional and local structures to Mount Pinatubo activity, in *Fire and Mud: Eruptions*
737 *and Lahars of Mount Pinatubo, Philippines*, edited by C. G. Newhall and R. S.
738 Punongbayan, pp. 351-370, Philippine Institute of Volcanology and Seismology,
739 Quezon City, and University of Washington Press, Seattle and London.

740 Byerlee, J. D. (1978), Friction of rocks, *Pure Appl. Geophys., 116*, 615-626.

741 Coombs, M. L., and J. E. Gardner (2001), Shallow-storage conditions for the rhyolite of
742 the 1912 eruption at Novarupta, Alaska, *Geology, 29*, 775-778.

743 Cornet, F. H., and B. Valette (1984), In situ stress determination from hydraulic injection
744 test data, *J. Geophys. Res., 89*, 11527-11537.
745 Cowee, C., J. F. Larsen, H. Geutschow, J. Eichelberger, A. Kent, and I. Hutcheon (1999),
746 Melt inclusion textures and volatile compositions from Novarupta Dome, Katmai
747 National Park, Alaska, *Eos Trans. AGU, 80*, Spring Meet. Suppl., S353.
748 Druitt, T.H., and R. S. J. Sparks (1984), On the formation of calderas during ignimbrite
749 eruptions, *Nature, 310*, 679-681.
750 Druitt, T. H., and C. R. Bacon C.R. (1986), Lithic breccia and ignimbrite erupted during
751 the collapse of Crater Lake Caldera, Oregon, *J. Volcanol. Geotherm. Res., 29*, 1-32.
752 Filson, J., T. Simkin, and L.-K. Leu (1973), Seismicity of a caldera collapse: Galapagos
753 Islands 1968, *J. Geophys. Res., 78*, 8591-8622.
754 Folch, A., and J. Martí (1998), The generation of overpressure in felsic magma chambers
755 by replenishment, *Earth Planet. Sci. Lett., 163*, 301-314.
756 Furuya M., S. Ohkubo, W. Sun, Y. Tanaka, J. Oikawa, and H. Watanabe (2003),
757 Spatiotemporal gravity changes at Miyakejima volcano, Japan: caldera collapse,
758 explosive eruptions and magma movement, *J. Geophys. Res.*, *108*,
759 10.1029/2002JB001989
760 Geshi, N., T. Shimano, T. Chiba, and S. Nakada (2002), Caldera collapse during the 2000
761 eruption of Miyakejima volcano, Japan, *Bull. Volcanol., 64*, 55-68.
762 Hess, K.-U., and D. B. Dingwell (1996), Viscosities of hydrous leucogranitic melts: a
763 non-Arrhenian model, *Am. Mineral., 81*, 1297-1300.

764 Hildreth, W. (2004), Volcanological perspectives on Long Valley, Mammoth Mountain,
765 and Mono Craters: several contiguous but discrete systems, *J. Volcanol. Geotherm.*
766 *Res., 136*, 169-198.
767 Hildreth, W., and J. Fierstein (2000), Katmai volcanic cluster and the great eruption of
768 1912, *Geol. Soc. Am. Bull., 112*, 1594-1620.
769 Hoblitt, R. P., E. W. Wolfe, W. E. Scott, M. R. Couchman, J. S. Pallister, and D. Javier
770 (1996), The preclimactic eruptions of Mount Pinatubo, June 1991, in *Fire and Mud:*
771 *Eruptions and Lahars of Mount Pinatubo, Philippines*, edited by C. G. Newhall and R.
772 S. Punongbayan, pp. 457-511, Philippine Institute of Volcanology and Seismology,
773 Quezon City, and University of Washington Press, Seattle and London.
774 Huppert, H. E., and A. W. Woods (2002), The role of volatiles in magma chamber
775 dynamics, *Nature, 420*, 493-495.
776 Irwan, M., F. Kimata, N. Fujii, S. Nakano, H. Watanabe, S. Sakai, M. Ukawa, E. Fujita,
777 and K. Kawai (2003), Rapid ground deformation of the Miyakejima volcano on 26-27
778 June 2000 detected by kinematic GPS analysis, *Earth Planets Space*, *55*, e13-e16.
779 Jones, J. W., and C. G. Newhall (1996), Preeruption and posteruption digital-terrain
780 models of Mount Pinatubo, in *Fire and Mud: Eruptions and Lahars of Mount Pinatubo,*
781 *Philippines*, edited by C. G. Newhall and R. S. Punongbayan, pp. 571-582, Philippine
782 Institute of Volcanology and Seismology, Quezon City, and University of Washington
783 Press, Seattle and London.
784 Kaneko, T., A. Yasuda, T. Shimano, S. Nakada, T. Fujii, T. Kanazawa, A. Nishizawa,
785 and Y. Matsumoto (2005), Submarine flank eruption preceding caldera subsidence
786 during the 2000 eruption of Miyakejima volcano, Japan, *Bull. Volcanol., 67*, 243-253.

787 Kazahaya, K., Y. Nakahori, H. Mori, H. Iino, M. Miyashita, J. Hirabayashi, H.
788 Shinohara, K. Uto, and M. Odai (2004), Gigantic SO_2 emission from Miyakejima
789 volcano, Japan, caused by caldera collapse, *Geology, 32*, 425-428.
790 Kennedy, B., and J. Stix (2003), Styles and mechanisms of caldera collapse, *Geosci.*
791 *Can., 30*, 59-72.
792 Kennedy, B., and J. Stix (2007), Magmatic processes associated with caldera collapse at
793 Ossipee ring dyke, New Hampshire, *Geol. Soc. Am. Bull., 119*, 3-17.

794 Kennedy, B., J. Stix, J. W. Vallance, Y. Lavallée, and M.-A. Longpré (2004), Controls on
795 caldera structure: results from analogue sandbox modeling, *Geol. Soc. Am. Bull., 116*,
796 515-524.
797 Khitarov, N. I., Ye. B. Lebedev, A. B. Slutskin, A. M. Dorfman, I. A. Soldatov, and N. I.
798 Revin (1976), The pressure dependence of the viscosity of basalt melts, *Geochem. Intl.,*
799 *13*(5), 126-133.
800 Kikuchi, M., Y. Yamanaka, and K. Koketsu (2001), Source process of the long-period
801 seismic pulses associated with the 2000 eruption of Miyake-jima volcano, and its
802 implications, *J. Geogr., 110*, 204-216.
803 Kobayashi, T., T. Ohminato, and Y. Ida (2003), Earthquake series preceding very long
804 period seismic signals, observed during the 2000 Miyakejima volcanic activity,
805 *Geophys. Res. Lett., 30*(8), 1423, doi:10.1029/2002GL016631.
806 Koyaguchi, T., and M. Ohno (2001), Reconstruction of eruption column dynamics on the
807 basis of grain size of tephra fall deposits 2. Application to the Pinatubo 1991 eruption,
808 *J. Geophys. Res., 106*, 6513-6533.
809 Kumagai, H., T. Ohminato, M. Nakano, M. Ooi, A. Kubo, H. Inoue, and J. Oikawa
810 (2001), Very-long-period seismic signals and caldera formation at Miyake Island,
811 Japan, *Science, 293*, 687-690.
812 Lavallée, Y., K.-U. Hess, B. Cordonnier, and D. B. Dingwell (2007), Non-Newtonian
813 rheological law for highly crystalline dome lavas, *Geology, 35*, 843-846.
814 Legros, F., K. Kelfoun, and J. Martí (2000), The influence of conduit geometry on the
815 dynamics of caldera-forming eruptions, *Earth Planet. Sci. Lett., 179*, 53-61.

816 Lowenstern, J. B. (1993), Evidence for a copper-bearing fluid in magma erupted at the
817 Valley of Ten Thousand Smokes, Alaska, *Contrib. Mineral. Petrol., 114*, 409-421.
818 Martí, J., A. Folch, A. Neri, and G. Macedonio (2000), Pressure evolution during
819 explosive caldera-forming eruptions, *Earth Planet. Sci. Lett., 175*, 275-287.
820 Mori, J., D. Eberhart-Phillips, and D. H. Harlow (1996a), Three-dimensional velocity
821 structure at Mount Pinatubo: resolving magma bodies and earthquake hypocenters, in
822 *Fire and Mud: Eruptions and Lahars of Mount Pinatubo, Philippines*, edited by C. G.
823 Newhall and R. S. Punongbayan, pp. 371-382, Philippine Institute of Volcanology and
824 Seismology, Quezon City, and University of Washington Press, Seattle and London.
825 Mori, J., R. A. White, D. H. Harlow, P. Okubo, J. A. Power, R. P. Hoblitt, E. P. Laguerta,
826 A. Lanuza, and B. C. Bautista (1996b), Volcanic earthquakes following the 1991
827 climactic eruption of Mount Pinatubo: strong seismicity during a waning eruption, in
828 *Fire and Mud: Eruptions and Lahars of Mount Pinatubo, Philippines*, edited by C. G.
829 Newhall and R. S. Punongbayan, pp. 339-350, Philippine Institute of Volcanology and
830 Seismology, Quezon City, and University of Washington Press, Seattle and London.
831 Nakada, S., M. Nagai, T. Kaneko, A. Nozawa, and K. Suzuki-Kimata (2005),
832 Chronology and products of the 2000 eruption of Miyakejima volcano, Japan, *Bull.*
833 *Volcanol.*, *67*, 205-218.
834 Roche, O., and T. H. Druitt (2001), Onset of caldera collapse during ignimbrite eruptions,
835 *Earth Planet. Sci. Lett., 191*, 191-202.
836 Roche, O., T. H. Druitt, and O. Merle (2000), Experimental study of caldera formation, *J.*
837 *Geophys. Res., 105*, 395-416.

838 Rose, W. I., G. J. S. Bluth, and G. G. J. Ernst (2000), Integrating retrievals of volcanic
839 cloud characteristics from satellite remote sensors: a summary, *Phil. Trans. Royal. Soc.*
840 *Edinburgh, A358*, 1585-1606.
841 Rose, W. I., Y. Gu, I. M. Watson, T. Yu, G. J. S. Bluth, A. J. Prata, A. J. Krueger, N.
842 Krotkov, S. Carn, M. D. Fromm, D. E. Hunton, G. G. J. Ernst, A. A. Viggiano, T. M.
843 Miller, J. O. Balenthin, J. M. Reeves, J. C. Wilson, B. E. Anderson, and D. E. Flittner
844 (2003), The February-March 2000 eruption of Hekla, Iceland from a satellite
845 perspective, *Am. Geophys. Union Geophys. Mon., 139*, 107-132.
846 Rutherford, M. J., and J. D. Devine (1996), Preeruption pressure-temperature conditions
847 and volatiles in the 1991 dacitic magma of Mount Pinatubo, in *Fire and Mud: Eruptions*
848 *and Lahars of Mount Pinatubo, Philippines*, edited by C. G. Newhall and R. S.
849 Punongbayan, pp. 751-766, Philippine Institute of Volcanology and Seismology,
850 Quezon City, and University of Washington Press, Seattle and London.
851 Scaillet, B., F. Holtz, and M. Pichavant (1998), Phase equilibrium constraints on the
852 viscosity of silicic magmas, *J. Geophys. Res., 103*, 27257-27266.
853 Scott, W. E., R. P. Hoblitt, R. C. Torres, S. Self, Ma. M. L. Martinez, and T. Nillos, Jr.
854 (1996) Pyroclastic flows of the June 15, 1991, climactic eruption of Mount Pinatubo, in
855 *Fire and Mud: Eruptions and Lahars of Mount Pinatubo, Philippines*, edited by C. G.
856 Newhall and R. S. Punongbayan, pp. 545-570, Philippine Institute of Volcanology and
857 Seismology, Quezon City, and University of Washington Press, Seattle and London.
858 Simkin, T., and K. A. Howard (1970), Caldera collapse in the Galápagos Islands, 1968,
859 *Science, 169*, 429-437.

860 Smith, R.L. (1979), Ash-flow magmatism, in *Ash-Flow Tuffs, Geol. Soc. Am. Spec. Pap.,*
861 *180*, edited by C. E. Chapin and W. E. Elston, pp. 5-27.
862 Spieler, O., D. B. Dingwell, B. Scheu, J. Taddeucci, B. Kennedy, and U. Kueppers
863 (2004), The fragmentation threshold of pyroclastic rocks, *Earth Planet. Sci. Lett., 226*,
864 139-148.
865 Stein, D. J., and F. J. Spera (2002), Shear viscosity of rhyolite-vapor emulsions at
866 magmatic temperatures by concentric cylinder rheometry, *J. Volcanol. Geotherm. Res.,*
867 *113*, 243-258.
868 Stix, J., and M. P. Gorton (1993), Replenishment and crystallization in epicontinental
869 silicic magma chambers: Evidence from the Bandelier magmatic system. *J. Volcanol.*
870 *Geotherm. Res., 55*, 201-215.
871 Sunde, R., J. Stix, and B. Kennedy (2004), The effect of eruption rate on caldera
872 structure: analogue experiments, *Eos Trans. AGU, 85*(17), Jt. Assem. Suppl., Abstract
873 V43A-17.
874 Ueda, H., E. Fujita, M. Ukawa, E. Yamamoto, M. Irwan, and F. Kimata (2005), Magma
875 intrusion and discharge process at the initial stage of the 2000 activity of Miyakejima,
876 central Japan, inferred from tilt and GPS data, *Geophys. J. Int.*, *161*, 891-906.
877 Uhira, K., T. Baba, H. Mori, H. Katayama, and N. Hamada (2005), Earthquake swarms
878 preceding the 2000 eruption of Miyakejima volcano, Japan, *Bull. Volcanol., 67*, 219-
879 230.
880 Ukawa M., E. Fujita, E. Yamamoto, Y. Okada, and M. Kikuchi (2000), The 2000
881 Miyakejima eruption: Crustal deformation and earthquakes observed by the NIED
882 Miyakejima observation network, *Earth Planets Space*, *52*, xix-xxvi.

883 Wallace, P., and T. M. Gerlach (1994), Magmatic vapor source for sulfur dioxide
884 released during volcanic eruptions: evidence from Mount Pinatubo, *Science, 265*, 497-
885 499.
886 Wallace, P. J., A. T. Anderson Jr., and A. M. Davis (1995), Quantification of pre-eruptive
887 exsolved gas contents in silicic magmas, *Nature, 377*, 612-616.
888 Wallace, P. J., Anderson Jr., and A. M. Davis (1999), Gradients in H_2O, CO_2, and
889 exsolved gas in a large-volume silicic magma system: Interpreting the record preserved
890 in melt inclusions from the Bishop Tuff, *J. Geophys. Res., 104*, 20097-20122.
891 Westrich, H. R., J. C. Eichelberger, and R. L. Hervig (1991), Degassing of the 1912
892 Katmai magmas: *Geophys. Res. Lett., 18*, 1561-1564.
893 Yamaoka, K., M. Kawamura, F. Kimata, N. Fujii, and T. Kudo (2005), Dike intrusion
894 associated with the 2000 eruption of Miyakejima volcano, Japan, *Bull. Volcanol., 67*,
895 231-242.
896

Figure captions

Figure 1. Plot of cumulative energy released by large earthquakes during the (a) Katmai 1912, (b) Pinatubo 1991, and (c) Fernandina 1968 caldera-forming eruptions. The steplike patterns of energy released at Katmai and Pinatubo contrast with the progressive trend seen at Fernandina. Note the different time and energy scales for the three events. Energies were calculated as $\log E = 1.96\,M + 2.05$ where E is the energy in Joules and M the magnitude of the earthquake. Souces of data as follows: Katmai, *Abe* [1992]; Pinatubo, National Earthquake Information Center, http://earthquake.usgs.gov/regional/neic/; Fernandina, *Filson et al.* [1973].

Figure 2. Cumulative energy plots for (a) Katmai 1912 and (b) Pinatubo 1991, in which the diagrams have been made non-dimensional. Time plotted on the x axis is normalized relative to the duration of the climactic eruptions; for Katmai, the duration was 60 hours, while for Pinatubo the duration was ~8.8 hours. Cumulative energy released by large earthquakes is normalized relative to the total amount of cumulative energy liberated during and immediately after the climactic eruptions.

Figure 3. Plot of energies of VLP events, both individual and cumulative, recorded at Miyakejima in July and August 2000. Using the relationship between the seismic energy (Joules) and seismic moment (Nm) $\log E_s = \log M_0 - 4.3$, we can evaluate the released seismic energy of each VLP event. In this calculation, we used the seismic moment of 39 VLP signals listed in *Kikuchi et al.* [2001] and obtained the values for M_0 from their

Figure 9. Also shown are caldera volumes plotted as a function of time and shown as solid circles; data from *Geshi et al.* [2002].

Figure 4. Schematic diagram of piston subsidence (a) prior to caldera collapse (e.g., Katmai, Pinatubo) and (b) after an increment of collapse (e.g., Fernandina, Miyakejima). The aspect ratio is $R = H / D$. See Table 2 for symbology and text for equations.

Figure 5. Magma underpressure plotted as a function of bulk modulus of the magma for the Katmai, Pinatubo, and Fernandina eruptions. Typical rock shear strengths are also shown. See text for discussion.

Figure 6. Caldera subsidence plotted against evacuation rate. The amount of displacement is calculated using Equation (8). A range of evacuation rates is used based on published values of volumetric eruption rates. (a) Katmai 1912; (b) Pinatubo 1991.

Figure 7. Caldera subsidence at Fernandina as a function of (a) evacuation rate of magma and (b) the time interval before subsidence. The amount of displacement is calculated using Equation (8).

Table 1. Input values for modeling

Parameter	Katmai	Pinatubo	Fernandina	Miyakejima
Aspect ratio of caldera block, R (dimensionless)	2.0	2.4	0.31	1.9 - 3.8
Initial volume of magma reservoir, V_o (m^3)	1.3×10^{10}	5.0×10^9	2.2×10^9	3.7×10^{10}
Cross-sectional area of base of caldera block, A (m^2)	4.0×10^6	4.9×10^6	8.0×10^6	2.0×10^6
Duration of magma evacuation before caldera block begins to subside, T (s)	117,360	17,953	21,600	43,200 to 86,400
Magma evacuation rate, α ($m^3\ s^{-1}$)	2.8×10^4 to 2.2×10^5	1.2×10^5 to 3.6×10^5	3.0×10^3 to 6.7×10^3	4.5×10^1 to 1.7×10^2

Sources of data: Katmai, *Hildreth and Fierstein* [2000]; Pinatubo, *Hoblitt et al*. [1996], *Koyaguchi and Ohno* [2001], *Mori et al*. [1996a, 1996b], *Scott et al*. [1996]; Fernandina, *Simkin and Howard* [1970], *Filson et al*. [1973]; Miyakejima, *Kumagai et al.* [2001], *Geshi et al.* [2002], *Kobayashi et al.* [2003], *Irwan et al.* [2003], *Ueda et al.* [2005].

Table 2. Symbols used in equations

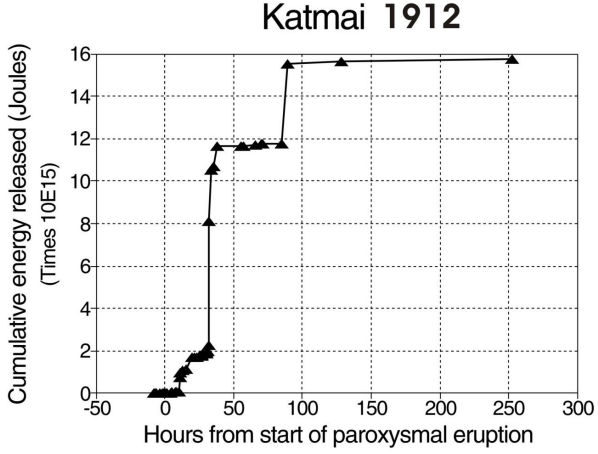
E	energy of volcanotectonic earthquake (J)
E_s	energy of VLP event (J)
M	magnitude of volcanotectonic earthquake
M_0	seismic moment of VLP event (N m)
A	cross-sectional area at the base of caldera block (m^2)
H	thickness of caldera block (m)
D	diameter of caldera block (m)
R	aspect ratio of caldera block, H/D (dimensionless)
z	displacement of caldera block (m)
V_o	initial volume of magma chamber prior to caldera subsidence (m^3)
ΔV	change in volume (m^3)
T	time between initiation of magma chamber evacuation and downward movement of caldera block (s)
α	evacuation rate of magma ($m^3\ s^{-1}$)
F_s	static friction (N)
F_d	dynamic friction (N)
p_o	original pressure in magma chamber (Pa)
p	pressure increase in magma chamber from downward movement of caldera block (Pa)
$p'T$	underpressure in magma chamber (Pa)
$p'T_{crit}$	critical magma underpressure to cause failure of caldera roof and initiate caldera collapse (Pa)
p'	rate of pressure decrease in magma chamber ($Pa\ s^{-1}$)
p_1	re-equilibrated pressure in magma chamber (Pa)
p_{lith}	lithostatic pressure (Pa)
Δp	pressure difference (Pa)
κ	bulk modulus of magma (Pa)
τ_c	critical shear stress for failure of caldera block (Pa)
τ_o	cohesion of caldera block (Pa)
σ_n	mean stress normal to the plane of failure (Pa)
μ	coefficient of internal friction of the caldera block (dimensionless)
k	constant (~0.6) (dimensionless)
ρ_r	density of caldera block ($kg\ m^{-3}$)
g	acceleration due to gravity ($m\ s^{-2}$)

Table 3. Downward displacement of the caldera block as a function of magma evacuation rate.

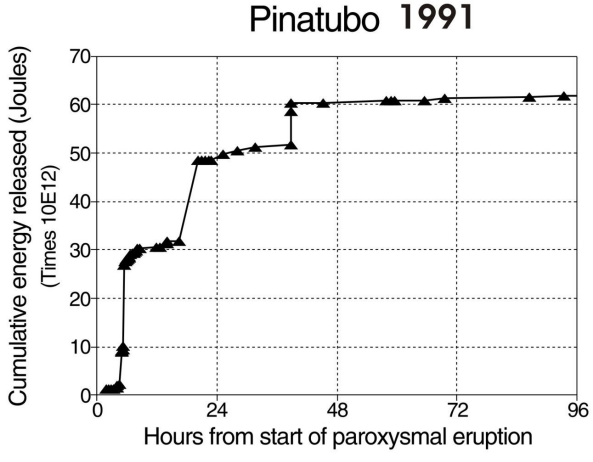
	Katmai		Pinatubo	
Parameter	Minimum	Maximum	Minimum	Maximum
Observed evacuation rate of magma (m^3 s^{-1})	2.8×10^4	2.2×10^5	1.2×10^5	3.6×10^5
Calculated displacement of the caldera block (m)	822	6484	440	1320
Observed surface displacement of the caldera block (m)	1200-1300		~900	

Sources of data: Katmai, *Hildreth and Fierstein* [2000]; Pinatubo, *Jones and Newhall* [1996], *Koyaguchi and Ohno* [2001], *Scott et al*. [1996].

(A)


Katmai 1912
Cumulative energy released (Joules)
(Times 10E15)
16
14
12
10
8
6
4
2
0
-50
0
50
100
150
200
250
300
Hours from start of paroxysmal eruption

(B)


Pinatubo 1991
Cumulative energy released (Joules)
(Times 10E12)
70
60
50
40
30
20
10
0
0
24
48
72
96
Hours from start of paroxysmal eruption

(C)

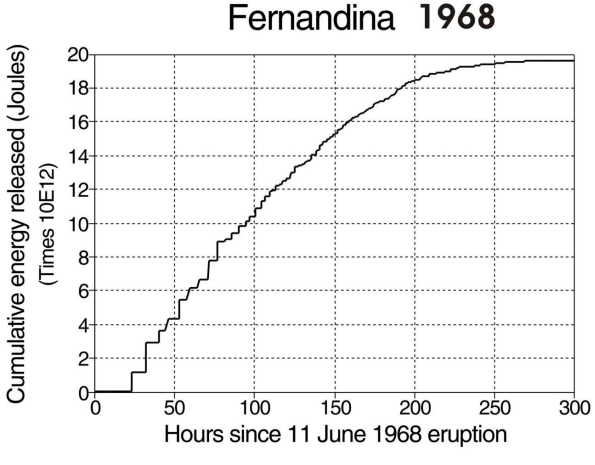
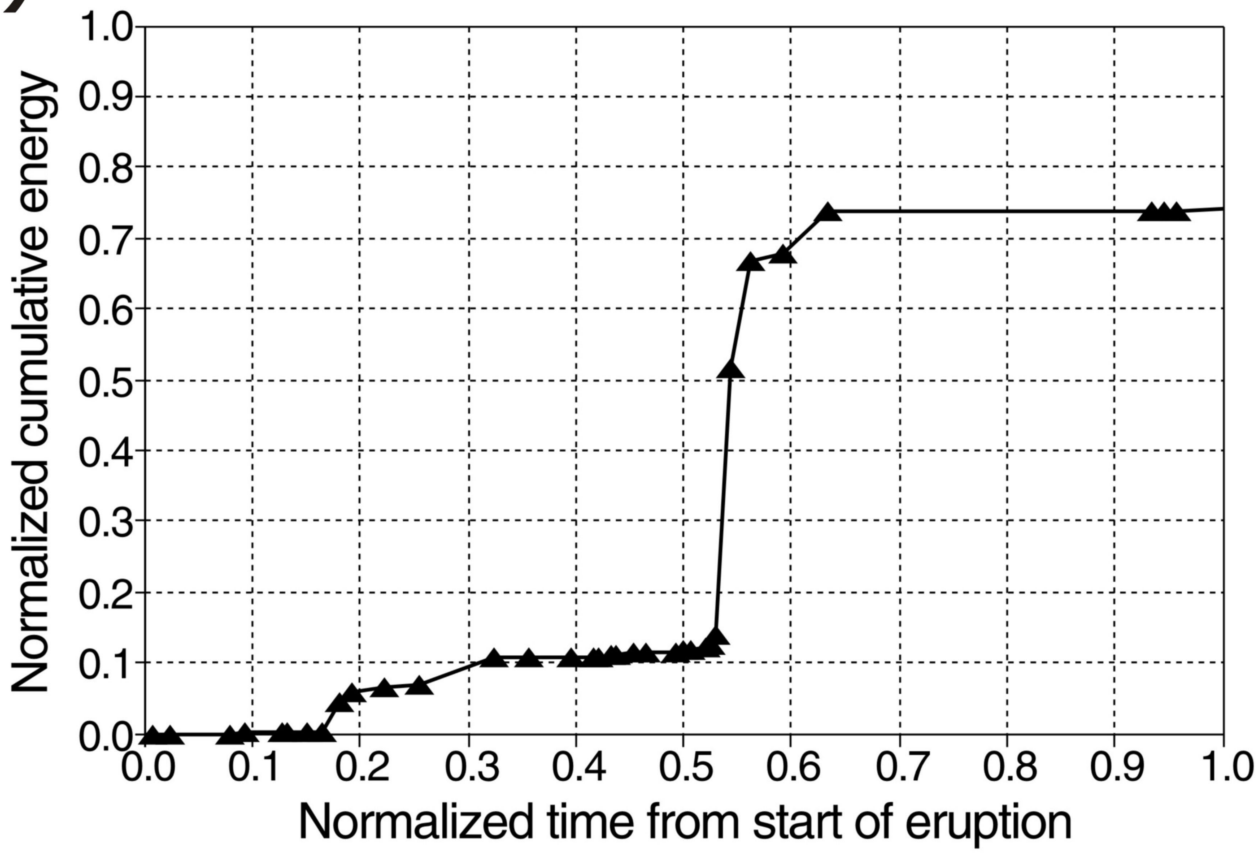

Fernandina 1968
Cumulative energy released (Joules)
(Times 10E12)
20
18
16
14
12
10
8
6
4
2
0
0
50
100
150
200
250
300
Hours since 11 June 1968 eruption

Fig. 1

(A)


Katmai
Normalized cumulative energy
Normalized time from start of eruption
0.0
0.1
0.2
0.3
0.4
0.5
0.6
0.7
0.8
0.9
1.0

(B)

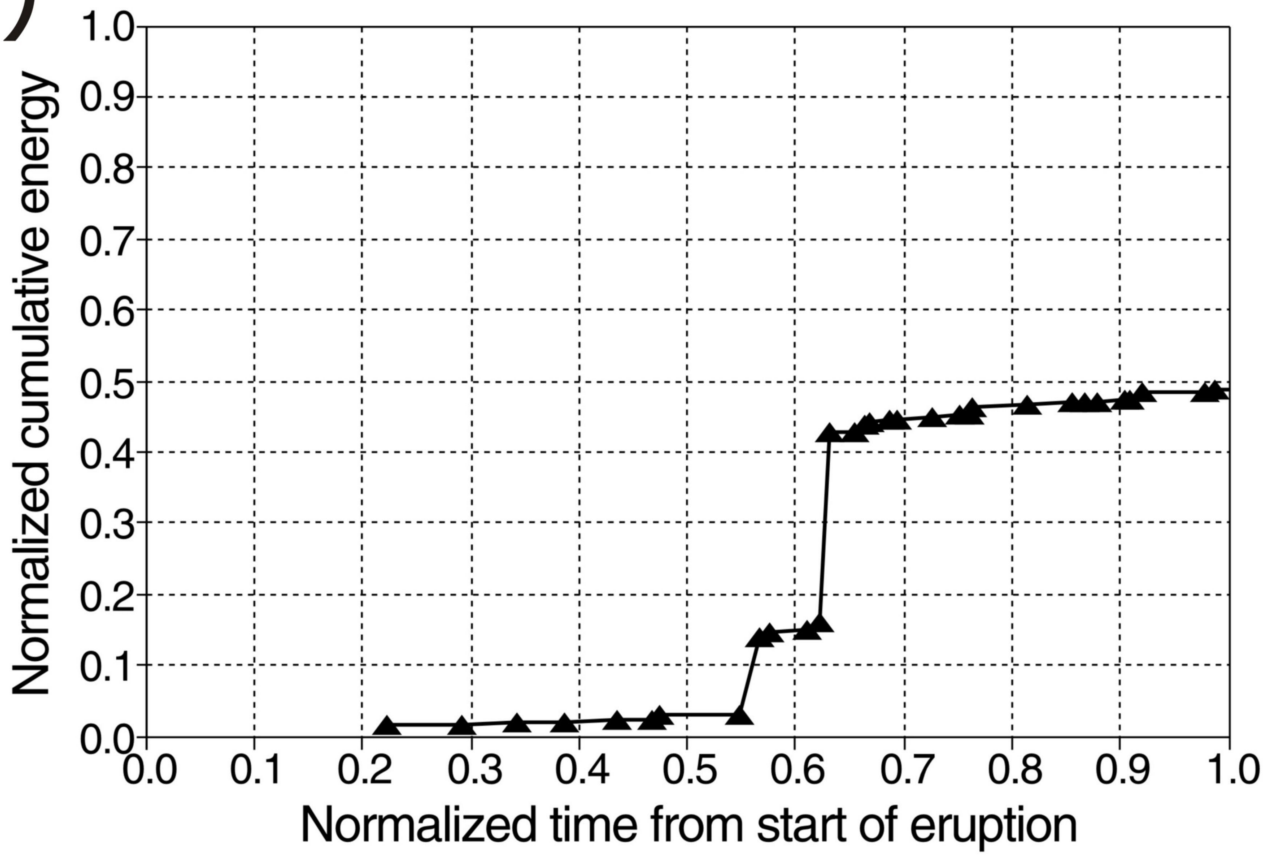

Pinatubo
Normalized cumulative energy
Normalized time from start of eruption
0.0
0.1
0.2
0.3
0.4
0.5
0.6
0.7
0.8
0.9
1.0

Fig. 2

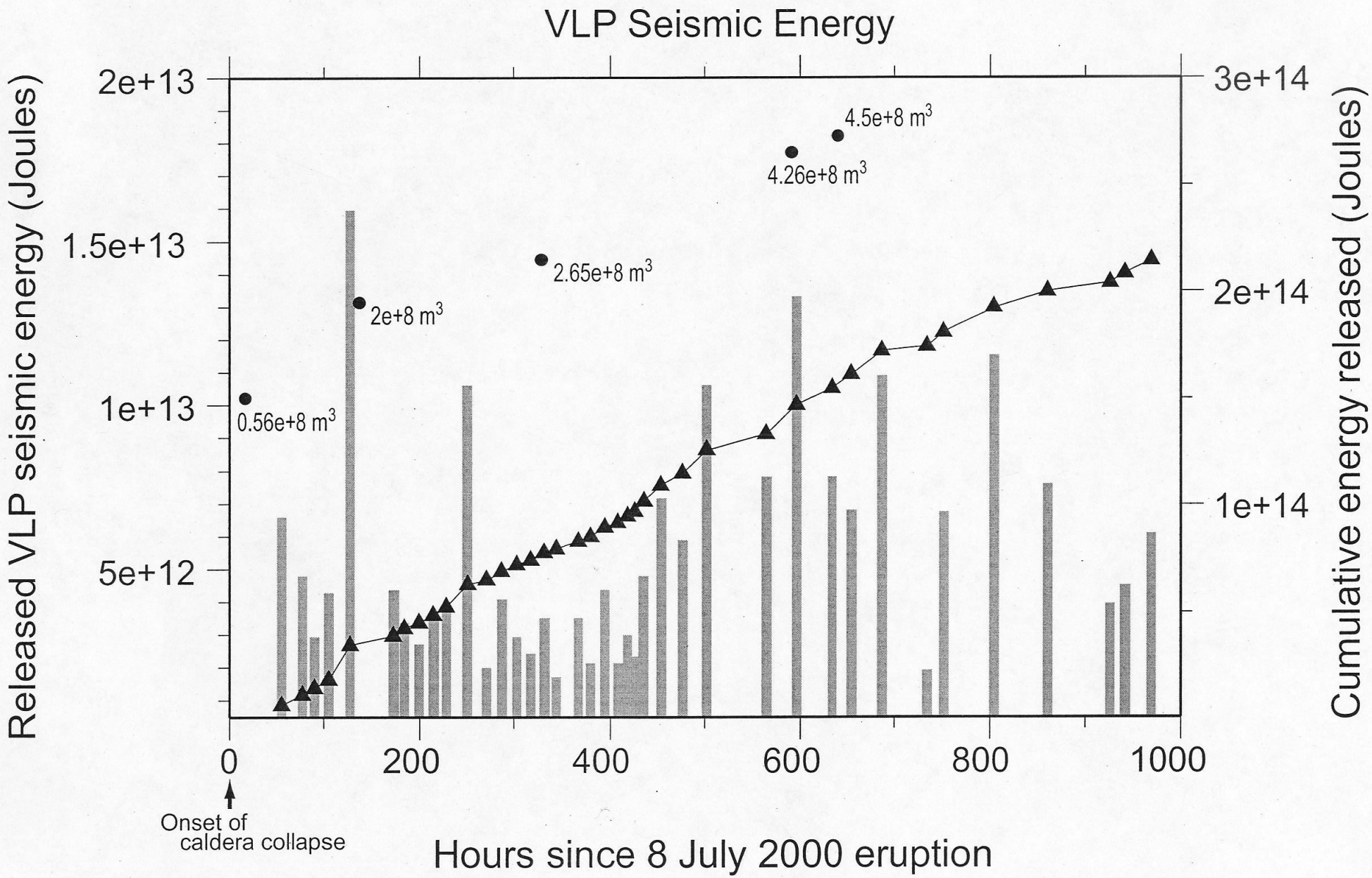

VLP Seismic Energy
Released VLP seismic energy (Joules)
Cumulative energy released (Joules)
2e+13
1.5e+13
1e+13
5e+12
3e+14
2e+14
1e+14
0.56e+8 m3
2e+8 m3
2.65e+8 m3
4.26e+8 m3
4.5e+8 m3
0
200
400
600
800
1000
Onset of caldera collapse
Hours since 8 July 2000 eruption

Fig. 3

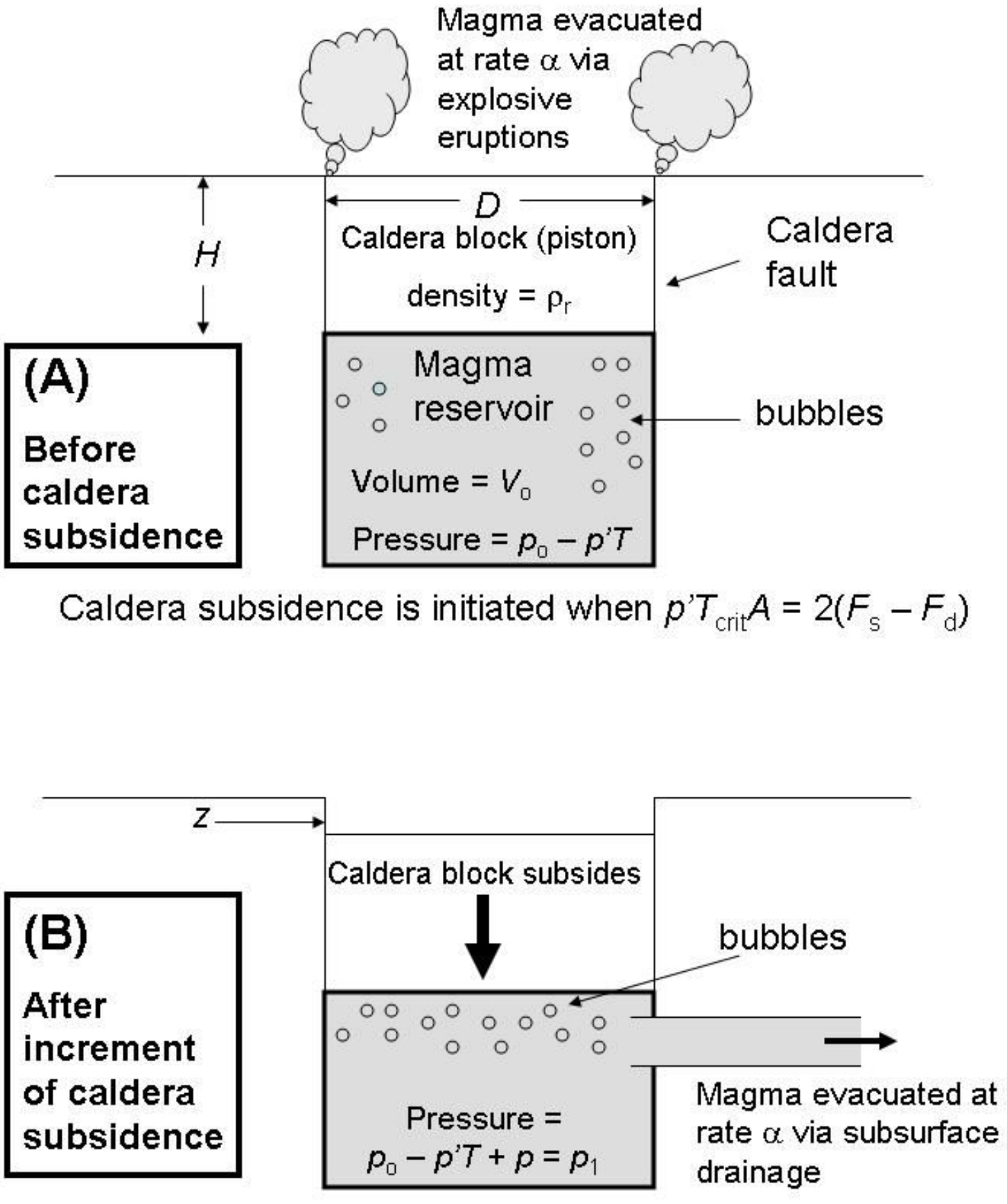

Magma evacuated at rate α via explosive eruptions
H
D
Caldera block (piston)
density = ρr
Caldera fault
(A)
Before caldera subsidence
Magma reservoir
bubbles
Volume = V0
Pressure = p0 – p'T
Caldera subsidence is initiated when p'Tcrit A = 2(Fs – Fd)
z
Caldera block subsides
(B)
After increment of caldera subsidence
bubbles
Pressure = p0 – p'T + p = p1
Magma evacuated at rate α via subsurface drainage

Fig. 4

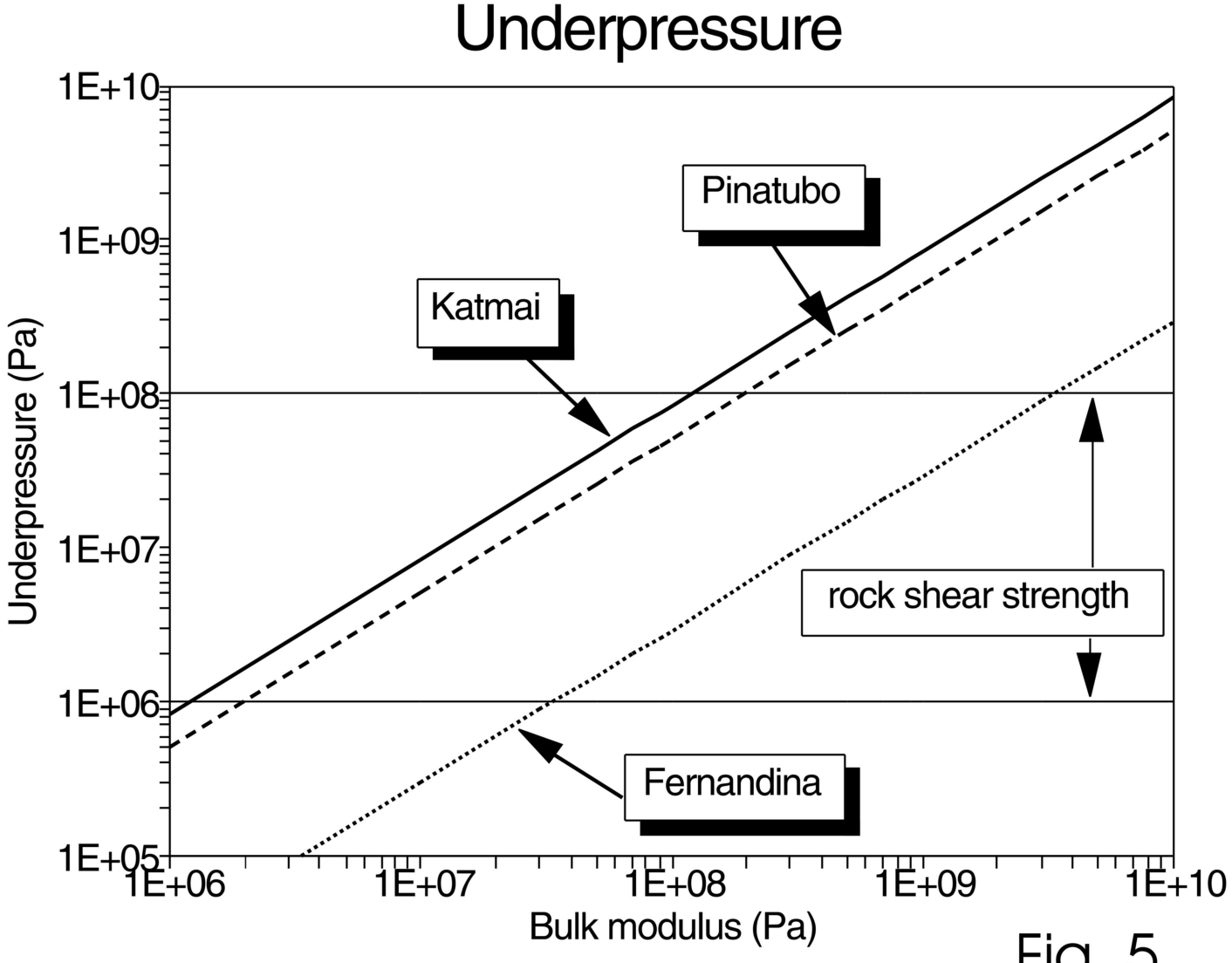
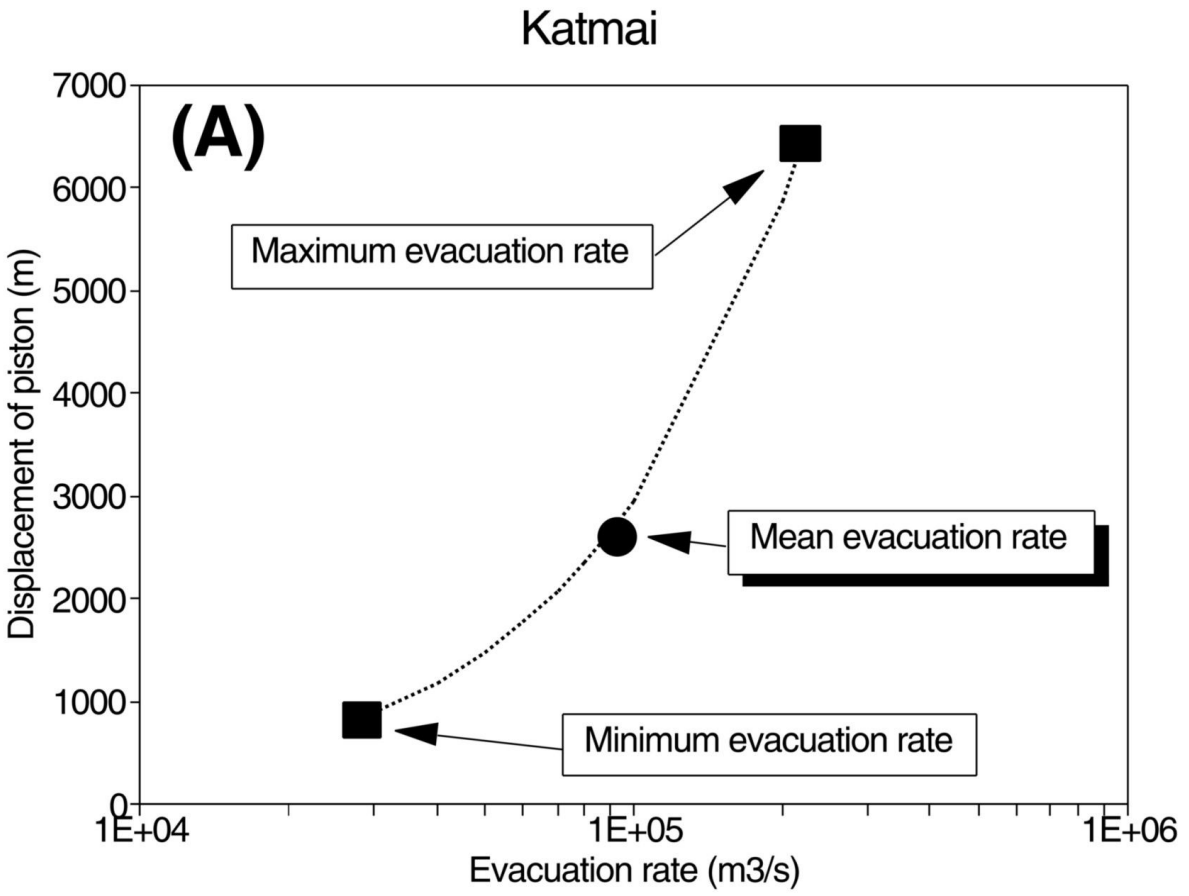

Underpressure
1E+10
1E+09
1E+08
1E+07
1E+06
1E+05
Underpressure (Pa)
Pinatubo
Katmai
rock shear strength
Fernandina
1E+06
1E+07
1E+08
1E+09
1E+10
Bulk modulus (Pa)

Fig. 5


Katmai
(A)
Maximum evacuation rate
Mean evacuation rate
Minimum evacuation rate
Displacement of piston (m)
7000
6000
5000
4000
3000
2000
1000
0
1E+04
1E+05
1E+06
Evacuation rate (m3/s)

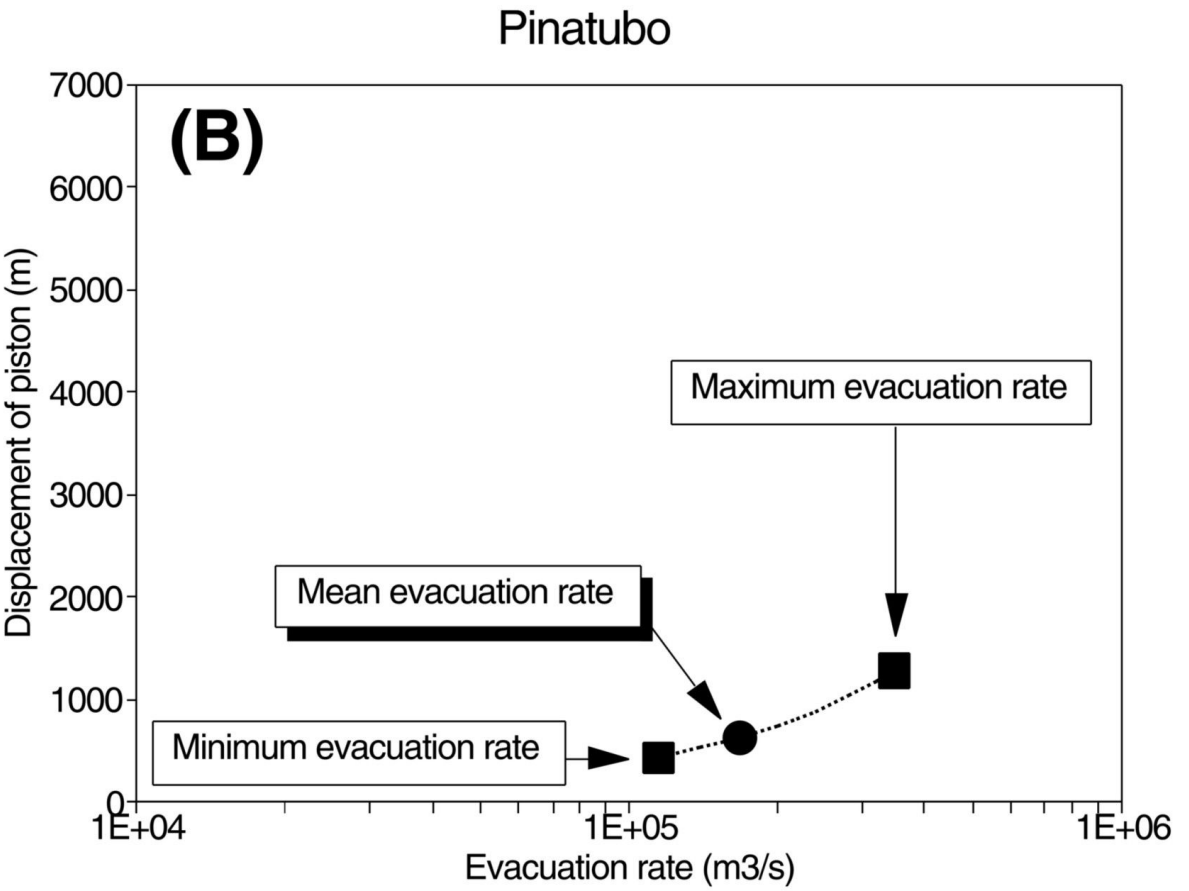
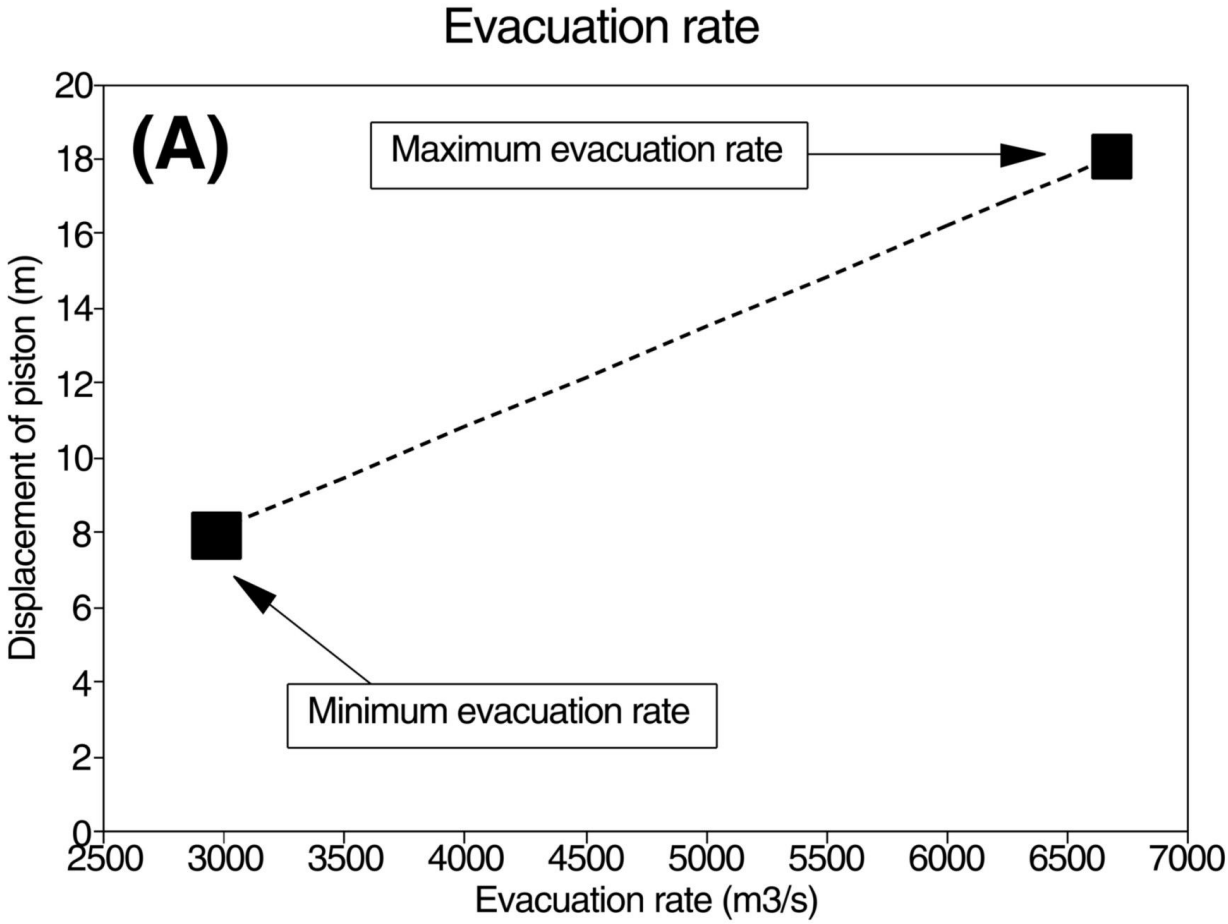

Pinatubo
(B)
Maximum evacuation rate
Mean evacuation rate
Minimum evacuation rate
Displacement of piston (m)
7000
6000
5000
4000
3000
2000
1000
0
1E+04
1E+05
1E+06
Evacuation rate (m3/s)

Fig. 6


Evacuation rate
(A)
Maximum evacuation rate
Minimum evacuation rate
Displacement of piston (m)
Evacuation rate (m3/s)
0
2
4
6
8
10
12
14
16
18
20
2500
3000
3500
4000
4500
5000
5500
6000
6500
7000

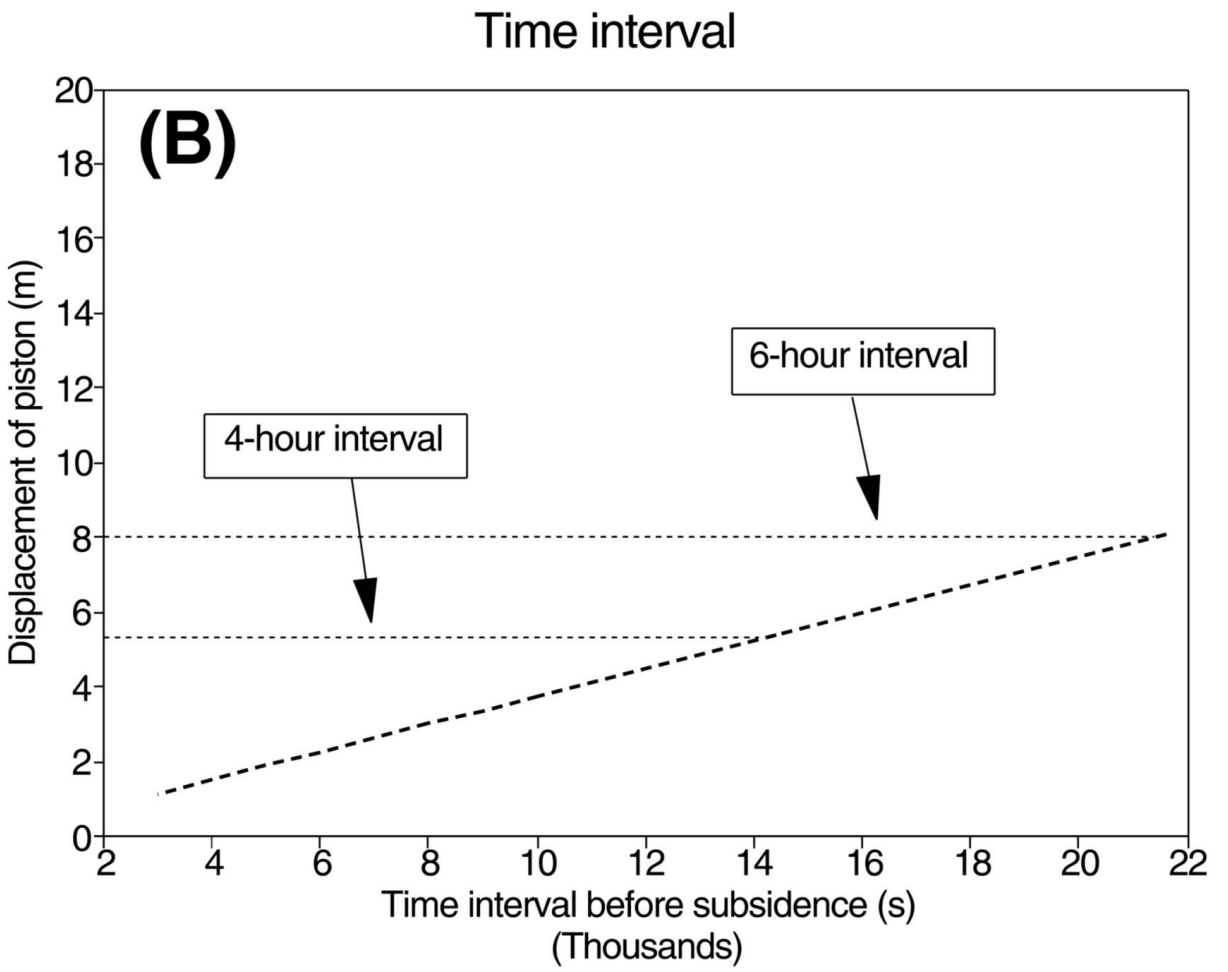

Time interval
(B)
6-hour interval
4-hour interval
Displacement of piston (m)
Time interval before subsidence (s)
(Thousands)
0
2
4
6
8
10
12
14
16
18
20
2
4
6
8
10
12
14
16
18
20
22

Fig. 7